REPORT DOCUMENTATION PAGE

Form Approved
OMB NO. 0704-0188

1. AGENCY USE ONLY (Leave Blank)	2. REPORT DATE	3. REPORT TYPE AND DATES COVERED
	July 2009	Reprint

4. TITLE AND SUBTITLE
Interference Rejection and Management

5. FUNDING NUMBERS
W911NF0410224 (46637CIMUR)

6. AUTHOR(S)
A. Batra, J.R. Zeidler, J.G.Proakis and L.B. Milstein

7. PERFORMING ORGANIZATION NAME(S) AND ADDRESS(ES)
University of California San Diego
9500 Gilman Drive, La Jolla, CA 92093-0407

8. PERFORMING ORGANIZATION REPORT NUMBER
N/A

9. SPONSORING / MONITORING AGENCY NAME(S) AND ADDRESS(ES)
U. S. Army Research Office
P.O. Box 12211
Research Triangle Park, NC 27709-2211

10. SPONSORING / MONITORING AGENCY REPORT NUMBER
N/A

11. SUPPLEMENTARY NOTES
The views, opinions and/or findings contained in this report are those of the author(s) and should not be construed as an official Department of the Army position, policy or decision, unless so designated by other documentation.

12 a. DISTRIBUTION / AVAILABILITY STATEMENT
Approved for public release; distribution unlimited.

12 b. DISTRIBUTION CODE
N/A

13. ABSTRACT (Maximum 200 words)

In this chapter, we consider interference suppression in several different wireless communication systems. The first topic treated is self-interference encountered among cooperating systems, for example, the self-interference that is encountered in cognitive radio systems and ultra-wideband (UWB) communication systems. Both single-carrier, direct sequence signals and multicarrier signals are considered, and the effects of the interference on the performance of a direct sequence UWB system that employs channel state estimation in the presence of the interference is evaluated. The second topic that is treated is the mitigation of narrowband interference in block-modulated multicarrier systems. Two schemes, multicarrier code-division multiple access (MC-CDMA) and orthogonal frequency division multiplexing (OFDM), are investigated. The inherent frequency diversity of MC-CDMA throug the use of spreading codes allows for robustness against interference. Conversely, OFDM must employ a signal processing technique to suppress the interference due to its lack of frequency diversity. The performance of OFDM is improved with the addition of forward error correction (FEC) coding in the frequency domain, thereby providing the system with frequency diversity. The third topic is the suppression of interference in multiple-input, multiple output (MIMO) wireless communication systems that employ multiple-transmit and multiple-receive antennas to increase the data rate and achieve signal diversity in fading multipath channels. Interference in MIMO wireless communication systems usually consists of intersymbol interference (ISI) due to channel multipath dispersion and cross-talk, or interchannel interference, due to the simultaneous transmissions from the multiple-transmit antennas

14. SUBJECT TERMS	15. NUMBER OF PAGES
N/A	34
	16. PRICE CODE: N/A

17. SECURITY CLASSIFICATION OR REPORT	18. SECURITY CLASSIFICATION ON THIS PAGE	19. SECURITY CLASSIFICATION OF ABSTRACT	20. LIMITATION OF ABSTRACT
UNCLASSIFIED	**UNCLASSIFIED**	**UNCLASSIFIED**	**UL**

NSN 7540-01-280-5500

Standard Form 298 (Rev.2-89)
Prescribed by ANSI Std. 239-18
298-102

Chapter 9
Interference Rejection and Management

Arun Batra, James R. Zeidler, John G. Proakis, and Laurence B. Milstein

9.1 Introduction

In this chapter, we consider interference suppression in several different wireless communication systems. The first topic treated is self-interference encountered among cooperating systems, for example, the self-interference that is encountered in cognitive radio systems and ultra-wideband (UWB) communication systems. Both single-carrier, direct sequence signals and multicarrier signals are considered, and the effects of the interference on the performance of a direct sequence UWB system that employs channel state estimation in the presence of the interference is evaluated.

The second topic that is treated is the mitigation of narrowband interference in block-modulated multicarrier systems. Two schemes, multicarrier code-division multiple access (MC-CDMA) and orthogonal frequency division multiplexing (OFDM), are investigated. The inherent frequency diversity of MC-CDMA through

Arun Batra
Department of Electrical and Computer Engineering, University of California, San Diego, La Jolla, CA 92093-0407, USA.
e-mail: abatra@ucsd.edu

James R. Zeidler
Department of Electrical and Computer Engineering, University of California, San Diego, La Jolla, CA 92093-0407, USA.
e-mail: zeidler@ece.ucsd.edu

John G. Proakis
Department of Electrical and Computer Engineering, University of California, San Diego, La Jolla, CA 92093-0407, USA.
e-mail: jproakis@ucsd.edu

Laurence B. Milstein
Department of Electrical and Computer Engineering, University of California, San Diego, La Jolla, CA 92093-0407, USA.
e-mail: milstein@ece.ucsd.edu

V. Tarokh (ed.), *New Directions in Wireless Communications Research*,
DOI 10.1007/978-1-4419-0673-1_9,

the use of spreading codes allows for robustness against interference. Conversely, OFDM must employ a signal processing technique to suppress the interference due to its lack of frequency diversity. The performance of OFDM is improved with the addition of forward error correction (FEC) coding in the frequency domain, thereby providing the system with frequency diversity.

The third topic is the suppression of interference in multiple-input, multiple-output (MIMO) wireless communication systems that employ multiple-transmit and multiple-receive antennas to increase the data rate and achieve signal diversity in fading multipath channels. Interference in MIMO wireless communication systems usually consists of intersymbol interference (ISI) due to channel multipath dispersion and cross-talk, or interchannel interference, due to the simultaneous transmissions from the multiple-transmit antennas. The focus of the section is on point-to-multipoint (broadcast) MIMO systems in which the channel characteristics are assumed to be known at the transmitter, so that interference mitigation can be performed at the transmitter.

9.2 Self-Interference Among Cooperating Systems

This section is concerned with the operation of systems that have been specifically designed to operate in the same frequency band as do other, preexisting, systems. Such overlay-type operations are often referred to as dynamic spectrum allocation. Because the spectral bands are the same for both systems, some type of interference suppression and/or interference avoidance is typically necessary. Further, the presence of the interference makes virtually all standard system functions, such as synchronization and diversity combining, less accurate. In Section 9.2.1, a brief overview of waveform design appropriate for overlay systems is presented, and in Section 9.2.2, the effects of overlaid interference, both with and without interference suppression at the receiver, on the accuracy of channel state information is presented.

9.2.1 Interference Suppression to Enable Spectrum Sharing

A fairly recent goal is to allow multiple classes of users to share common spectrum in order to increase the spectral efficiency in whatever band is under consideration. This has led to technologies such as cognitive radio and ultra wideband communications, which have the characteristics of enabling secondary users to share spectrum with primary users, providing the former set of users do not impose excessive interference on the latter set. Such scenarios typically, require the use of interference suppression and management techniques.

This involves the design and analysis of spectrum sensing techniques in order to determine where and when primary users are present. It also involves

choosing appropriate waveform designs, such as single-carrier DS or multicarrier techniques (e.g., multicarrier DS), and combining them with appropriate signal processing schemes to enable them to both withstand the affects of overlaid interference and intentional jamming and minimize the interference they impose on the overlaid waveforms. For the latter case, the signal processing will take the form of placing appropriate notches in the spectrum of the transmitted DS signals at frequency locations where the spectrum sensing operation indicated that preexisting narrowband users were active. In the former case, the signal processing can again take the form of notch filtering, but now at the DS receivers. In other words, notch filtering at the DS transmitters is designed to protect the overlaid users and notch filtering at the DS receivers is designed to protect the DS signals themselves. Also, the term "notching" is used in a general sense, meaning that, for example, in the case of multicarrier DS, the notching might imply simply not transmitting appropriate subcarriers. Note that the interaction of channel estimation errors (such as those incurred while performing tasks such as spectral sensing and channel state estimation) and interference/jamming is an important consideration and is discussed below.

9.2.1.1 Single-Carrier Direct Sequence

Adaptive MMSE receivers: As is well known, a Wiener filter can greatly improve the performance of DS receivers in the presence of narrowband interference. Based on the a priori knowledge of the channel and narrowband interference (NBI) statistics, a Wiener filter is able to suppress NBI and obtain a good estimate of the channel realization. For instance, the frequency response of a Wiener filter is presented in Section 9.2.2 for different NBI levels, and it will be seen that the filter suppresses the frequencies where the NBI is located. In practice, the channel and narrowband interference statistics are not known and might be changing with time. Therefore, the Wiener filter must be made adaptive. As shown in [49, 53], the LMS filter is very effective in rejecting NBI when the ratio of the NBI bandwidth to the signal bandwidth is small, assuming the LMS filter has had sufficient time to converge.

Tunable notch filters: There are many examples in the literature that illustrate the usefulness of notch filters when trying to suppress narrowband interference. For example, it was shown in [33] that the presence of an interference rejection filter can significantly improve the acquisition system performance of a DS CDMA receiver. And it was shown in [34] that in order to successfully have a CDMA system overlay narrowband users, i.e., to deploy it in a manner such that neither set of users caused excessive interference to the other set, it was desirable to use tunable notch filters at both the CDMA transmitters and the CDMA receivers.

9.2.1.2 Multicarrier Direct Sequence

In a multicarrier DS system, multiple narrowband DS waveforms, each at a distinct carrier frequency, are combined to yield a composite wideband DS signal. Among

the advantages of such an approach is the ability to achieve the same type of system performance that a single-carrier DS signal would provide, such as diversity enhancement over a multipath channel; however, this is achieved without the need for a contiguous spectral band. It was shown in [9] that for an exponential multipath intensity profile and imperfect channel estimation, multicarrier DS systems outperform single-carrier DS systems.

In the multicarrier scenario, the receiver first operates in a spectrum sensing mode, detecting the presence and frequency occupancy of possible narrowband users, as well as possible jammers. Then, after appropriate subcarriers are excised, both channel estimation and data detection are performed.

9.2.2 Effects of Interference on Channel State Estimation

One of the key needs of wireless receivers is accurate channel state information (CSI) so that basic functions such as synchronization and diversity combining can be accomplished. In this section, we consider the problem of trying to achieve accurate CSI in the presence of external interference; we also look at the impact on system performance when either the estimation module or the data detection module at the receiver does not take sufficient measures to account for the interference. As a specific system with which to illustrate the concepts, we will use UWB.

Consider a direct sequence UWB system as described in [43, 44]. A block diagram of the low-pass equivalent receiver is shown in Fig. 9.1. The first block is a chip-matched filter which is perfectly synchronized to the desired waveform, and where binary phase-shift keying (BPSK) is the modulation format. The output of the matched filter is sampled at the chip rate, and the samples are then processed by a rake receiver. The received signal consists of the UWB waveform, additive white Gaussian noise (AWGN), and narrowband interference which is modeled as a wide-sense stationary Gaussian random process.

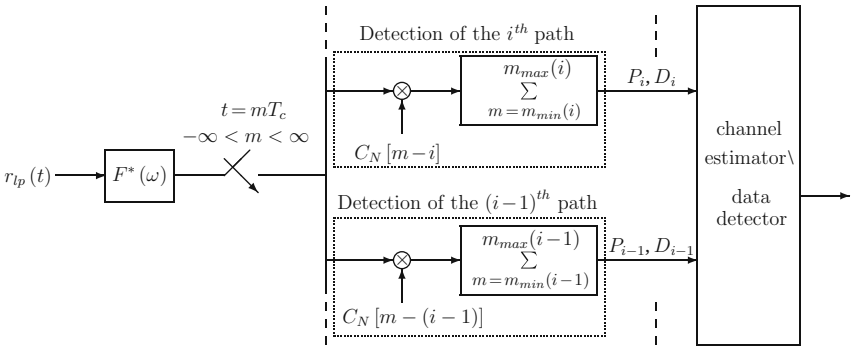

Fig. 9.1 Low-pass equivalent of the DS/CDMA receiver. For the reception of the νth data bit, $m_{\min}(i) = (\nu-1)N + i$ and $m_{\max}(i) = \nu N + i - 1$. For the νth channel estimation period, $m_{\min}(i) = (\nu-1)NN_p + i$ and $m_{\max}(i) = \nu NN_p + i - 1$. Note that N is the processing gain and N_P is the number of pilot symbols.

There are two types of receiver configurations that are studied. The first one is based upon simplicity of implementation: It uses a sample mean (SM) to estimate the gain of each resolvable path used in the rake receiver of Fig. 9.1 and combines those paths that are resolved using maximal-ratio combining (MRC). Note that neither the estimator nor the detector requires knowledge of the statistics of the channel, and neither of them make any explicit attempt to suppress the interference. The second receiver is more complex. It employs a minimum mean-squared error (MMSE) estimator and a maximum-likelihood (ML) detector. Thus, the second receiver requires knowledge of the second-order statistics of the interference, and those statistics typically are unknown at the receiver and thus requires an estimate. In what follows we assume that this latter information is available noise free.

A detailed analysis of this problem is presented in [43,44]. Here, we just describe some of the results in the context of the effect that the interference has in achieving accurate CSI. Consider first Fig. 9.2. The leftmost curve, labeled (I), displays the performance of the system when perfect CSI is available (i.e., we have a genie-aided receiver) and ML detection is used. This curve corresponds to interference-free conditions, and thus represents a lower bound on the performance of any of the other systems to be discussed. The three curves labeled (II) correspond to imperfect CSI and to signal-to-interference ratios (SIR) of -10, -15, and -20 dB. The receiver is an MMSE/ML, and we observe that, because this receiver has statistical knowledge of the interference, it can configure itself to suppress that interference. This will be

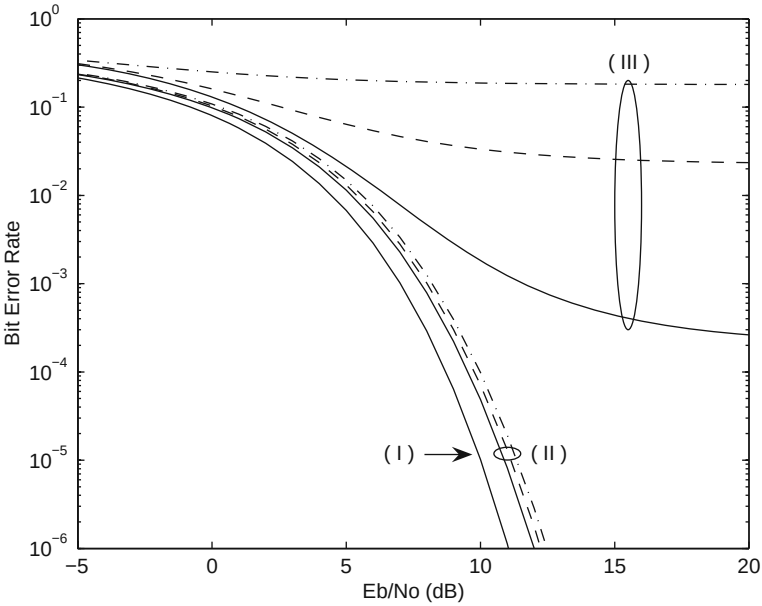

Fig. 9.2 Bit error rate for the DS/CDMA system: (I) perfect channel estimation and ML data detection in the absence of NBI, (II) MMSE/ML receiver, and (III) SM/MRC receiver. SIR $=$ -10 dB (*solid lines*), -15 dB (*dashed*), -20 dB (*dash-dot*). Number of training bits: 50

illustrated below and is the reason the latter three curves of Fig. 9.2 are so close to the interference-free curve.

If we replace the MMSE/ML receiver with an SM/MRC receiver, we get the performance curves shown in Fig. 9.2 that are labeled (III). Note that all three curves now experience an error floor, and that the performance of the curve with an SIR of -20 dB is virtually worthless, notwithstanding the fact that the system is operating with a processing gain of 127 (i.e., roughly 21 dB).

All the estimates used in the curves shown in Fig. 9.2 were made with a training sequence of 50 bits. To see the sensitivity of the system to the number of training bits, consider the curves shown in Fig. 9.3. As in Fig. 9.2, the leftmost curve corresponds to perfect CSI, the curves labeled (II) correspond to the MMSE/ML receiver, and the curves labeled (III) correspond to the SM/MRC receiver. For each of the latter two sets of curves, results are shown for observation intervals corresponding to 10, 30, and 50 bits. Once again, it is seen that the performance of the MMSE/ML receiver in the presence of channel estimation error is very close to the performance achievable with perfect CSI, whereas the performance of the SM/MRC receiver suffers tremendous degradation.

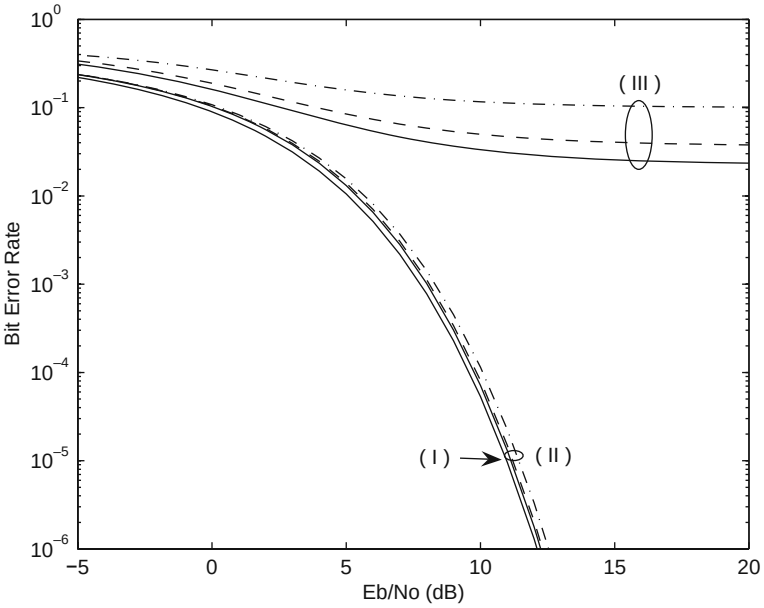

Fig. 9.3 Bit error rate for the DS/CDMA system: (I) perfect channel estimation and ML data detection, (II) MMSE/ML receiver, and (III) SM/MRC receiver. Number of training bits: 10 (*dash-dot lines*), 30 (*dashed*), 50 (*solid*). SIR $= -15$ dB

To obtain an intuitive feeling for what is taking place, consider the three curves shown in Fig. 9.4. All three correspond to the use of the MMSE/ML receiver, and all three show the transfer function of that receiver. A frequency range of -250 to $+250$ MHz is shown, and there is a narrowband Gaussian interferer located between

−20 and +20 MHz. The curves correspond to SIRs of −20 dB, −10 dB, and infinity (i.e., no interference). Note that the three curves virtually lie on top of one another over the entire frequency range shown, except for the region −20 to +20 MHz. In that region, it can be seen that the receiver is implementing a notch to suppress the interference (when it is present), and the depth of that notch is proportional to the strength of the interference.

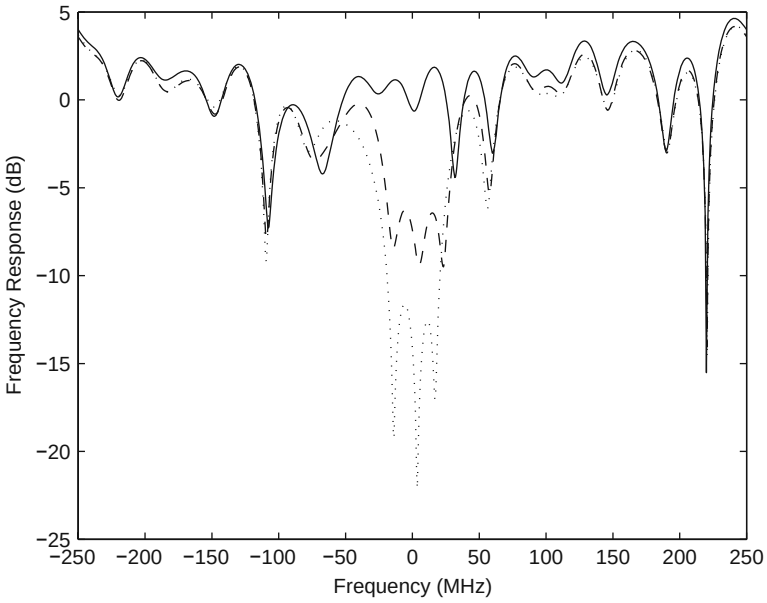

Fig. 9.4 Frequency response of the ML detector in the absence of NBI (*solid line*) and in the presence of NBI with SIR = −10 dB (*dashed line*) and −20 dB (*dotted line*). The NBI has 40 MHz of bandwidth and is centered at 0 Hz

9.3 Interference Mitigation in Block-Modulated Multicarrier Systems

In this section, two multicarrier schemes [7, 15], specifically multicarrier code-division multiple access (MC-CDMA) [10, 16, 23, 59] and orthogonal frequency division multiplexing (OFDM) [11, 54], are evaluated in the presence of narrowband interference (NBI). This interference can arise when other systems are occupying the same spectrum, as occurs naturally in the unlicensed bands [27] or from intentional jamming. This has led to the emergence of cognitive radio systems [35]. As discussed in the previous section, the transmitter and receiver of these systems must coordinate which frequencies are unaffected by the interference. For effective operation without cooperation, systems are limited to dealing with interference at the receiver, which is what is examined in this section.

MC-CDMA and OFDM are designed as block modulation schemes that convert an input into multiple low-rate streams that are transmitted on separate narrowband subcarriers, allowing the subcarriers to overlap orthogonally in frequency, thereby providing an increase in spectral efficiency. This design also allows the bandwidth of each subcarrier to approximate the coherence bandwidth of the channel, ensuring that each tone experiences flat fading. This also simplifies the equalization process at the receiver. These systems fit naturally in the context of cognitive radios because they have the ability to turn off subcarriers that are affected by interference [3]. In MC-CDMA, each subcarrier of a given user is multiplied by a single chip of a spreading sequence [39]. At the receiver, after demodulation of the subcarriers, the chips are then correlated with a locally generated chip sequence to provide the multiple-access capability. Conversely, OFDM does not spread the data symbols across the subcarriers. OFDM is thus a special case of MC-CDMA, in which the spreading codes are simply the columns of the identity matrix. The result of this is that uncoded OFDM does not provide frequency diversity.

These techniques differ from other wideband systems, such as direct sequence CDMA (DS-CDMA) and multicarrier direct sequence CDMA (MC-DS-CDMA) [13, 28], which were discussed in the previous section. For these modulations the bandwidth of the signal is greater than the coherence bandwidth of the channel, inducing frequency-selective fading. A rake [39] receiver can be used in addition to obtain path diversity, thereby reducing the deleterious effects of the frequency-selective multipath fading channel. A comparison of MC-DS-CDMA and MC-CDMA can be found in [15, 32].

The inherent frequency diversity of MC-CDMA allows for improved performance in interference-limited, frequency-selective channels [57]. Since OFDM lacks frequency diversity, it must employ signal processing and coding techniques to mitigate the interference. There has been a great deal of research concerning mitigation of NBI in an uncoded OFDM system. Proposed techniques range from using orthogonal codes [8, 21, 57], frequency-domain cancellation [14, 37], receiver windowing [41], and excision filtering [12]. More recently there has been some work relating to NBI suppression in coded OFDM systems [12, 45, 57].

In this work, the prediction-error filter (PEF) [30, 60] is selected for interference mitigation in OFDM. This is an example of excision filtering first described in [12]. First, this system is compared with MC-CDMA in an uncoded scenario. Then the addition of forward error correction coding for each system will be examined. In this case, OFDM will now also possess frequency diversity due to the coding across the subcarriers.

9.3.1 Interference Mitigation in an Uncoded Multicarrier System

A block diagram of the system model considered in this section is shown in Fig. 9.5. The code (spreading) matrix, $\mathbf{B}$, is an $N \times N$ unitary matrix whose columns contain the N spreading sequences. The kth column is responsible for spreading the kth

data symbol, D_k. Note that when $\mathbf{B}$ is the identity matrix (i.e., $\mathbf{B} = \mathbf{I}$), the system becomes identical to OFDM.

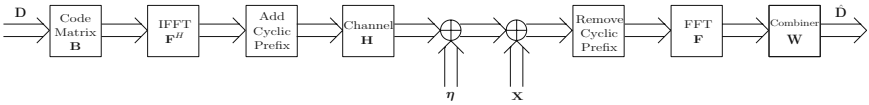

Fig. 9.5 Block diagram of uncoded MC-CDMA

The received signal is given by

$$\mathbf{Y}' = \mathbf{F}\left[\mathbf{H}\mathbf{F}^H\mathbf{B}\mathbf{D} + \mathbf{x} + \boldsymbol{\eta}\right], \tag{9.1}$$

where $\mathbf{F}$ is the $N \times N$ DFT matrix, $\mathbf{B}$ is the $N \times N$ code matrix, $\mathbf{D}$ is the $N \times 1$ vector of data symbols that is drawn from an arbitrary QAM constellation, $\mathbf{x}$ is an $N \times 1$ vector of interference samples, $\boldsymbol{\eta}$ is an $N \times 1$ vector of Gaussian noise samples, and $(\cdot)^H$ is the Hermitian (conjugate transpose) operator. Finally, $\mathbf{H}$ is the $N \times N$ channel matrix whose components are given by the taps of a multipath (frequency-selective) channel, as defined by the impulse response

$$h(t) = \sum_{l=0}^{L-1} h_l \delta(t - lT_s), \tag{9.2}$$

where L is the number of multipath components and T_S is the original symbol period. The channel coefficients, h_l, are i.i.d. zero-mean, circularly Gaussian random variables with variance

$$E\left[|h_l|^2\right] = \frac{1}{L} \quad \forall l, \tag{9.3}$$

where $E[\cdot]$ represents the expectation operator.

A cyclic prefix, composed of the last G samples of $\mathbf{F}^H\mathbf{D}$, is employed to mitigate the effects of intersymbol interference and intercarrier interference (ICI). When the length of the cyclic prefix is greater than the delay spread of the channel (L), linear convolution is equivalent to circular convolution and $\mathbf{H}$ is circulant. A well-known property of circulant matrices is that their eigenvectors are simply the columns of the DFT matrix [22]. Thus, (9.1) can be rewritten as follows:

$$\begin{aligned}\mathbf{Y}' &= \tilde{\mathbf{H}}\mathbf{B}\mathbf{D} + \mathbf{F}\mathbf{x} + \mathbf{F}\boldsymbol{\eta} \\ &= \tilde{\mathbf{H}}\mathbf{B}\mathbf{D} + \mathbf{X} + \mathbf{N},\end{aligned} \tag{9.4}$$

where $\tilde{\mathbf{H}}$ is an $N \times N$ diagonal matrix of the eigenvalues of $\mathbf{H}$. Coherent demodulation requires removing the phase of the channel, thus let $\tilde{\mathbf{H}}_\theta$ be a diagonal matrix containing the phase information of the channel, that is

$$\tilde{\mathbf{H}}_\theta = e^{j\angle\tilde{\mathbf{H}}}, \tag{9.5}$$

and let $\tilde{\mathbf{H}}_\rho$ be the magnitude of the eigenvalues, given as

$$\tilde{\mathbf{H}}_\rho = |\tilde{\mathbf{H}}| = \begin{bmatrix} \rho_0 & 0 & \cdots & 0 \\ 0 & \rho_1 & \cdots & 0 \\ \vdots & \vdots & \ddots & \vdots \\ 0 & 0 & \cdots & \rho_{N-1} \end{bmatrix}, \tag{9.6}$$

where ρ_k is a Rayleigh random variable. Note that $\tilde{\mathbf{H}} = \tilde{\mathbf{H}}_\theta \tilde{\mathbf{H}}_\rho$.

After coherent detection, the input to the combiner is given as

$$\mathbf{Y} = \tilde{\mathbf{H}}_\theta^H \mathbf{Y}' = \tilde{\mathbf{H}}_\rho \mathbf{B}\mathbf{D} + \tilde{\mathbf{H}}_\theta^H (\mathbf{X} + \mathbf{N}). \tag{9.7}$$

The interference samples in the time domain seen in (9.1) are given by

$$\begin{aligned} x_n &= \sqrt{E_x} e^{j(2\pi f_x n T_s + \theta)} \\ &= \sqrt{E_x} e^{j\left(\frac{2\pi}{N}(m+\alpha)n + \theta\right)}, \end{aligned} \tag{9.8}$$

where E_x is the interferer power and θ is a random phase distributed uniformly between $-\pi$ and π. The frequency of the interference, f_x, is defined as a function of the original sampling frequency, f_s, namely $f_x = (m+\alpha)\frac{f_s}{N}$. In this formulation of the interference, m represents the tone closest to the interference, while $\alpha \in [-0.5, 0.5]$ is the offset from tone m. The second line of (9.8) is obtained by noting that $f_s = \frac{1}{T_s}$.

The time-domain interference samples in (9.8) are converted into the frequency domain

$$X_k = [\mathbf{F}\mathbf{x}]_k = \sqrt{\frac{E_x}{N}} \frac{1 - e^{j2\pi\alpha}}{1 - e^{j\frac{2\pi}{N}(m+\alpha-k)}} e^{j\theta}, \tag{9.9}$$

where $[\cdot]_k$ is the kth component of the given vector. The result of (9.9) indicates that the interference per tone is dependent on the relative distance of tone k from the interferer frequency. This is referred to as spectral leakage, as the interference power is leaked into all of the tones. From (9.9), it can be seen that as the interference power increases, so does the number of tones that are significantly interfered with.

In the case of $\alpha = 0$, the interference is orthogonal to all the subcarriers other than the m^{th} subcarrier. The interference after the DFT reduces to

$$X_k = \begin{cases} \sqrt{N E_x} e^{j\theta}, & k = m \\ 0, & k \neq m \end{cases}. \tag{9.10}$$

Thus the interference is limited to tone m in this case.

Finally, the last term of (9.4), $\mathbf{N}$, is an $N \times 1$ vector of noise samples that have the same statistics as in the time domain.

9.3.1.1 MC-CDMA

The code matrix (**B**) employed in this work is defined component wise [36, 57] by

$$[B]_{kl} = \frac{1}{\sqrt{N}} e^{j\frac{2\pi}{N}kl}, \quad k, l = 0, \ldots, N-1. \tag{9.11}$$

Note that the code matrix is unitary, that is $\mathbf{B}\mathbf{B}^H = \mathbf{B}^H\mathbf{B} = \mathbf{I}_N$, where $\mathbf{I}_N$ is the $N \times N$ identity matrix. Another option that can be used for the orthogonal spreading codes, are the Walsh–Hadamard codes. However, note that these codes are only defined for lengths of $N = 2^n$, where n is an integer greater than zero [15].

The combiner weights required to extract the symbol vector, **D**, are derived under the minimum mean-square error (MMSE) criterion [57, 58] and obtained by solving the Wiener–Hopf equation

$$\mathbf{W} = \mathbf{R}_{YY}^{-1}\mathbf{R}_{YD}, \tag{9.12}$$

where $\mathbf{R}_{YY}$ is the autocorrelation matrix of the received signal and $\mathbf{R}_{YD}$ is the cross-correlation matrix between the received signal and the symbol vector, **D**. Assuming that all the received components are independent and that the channel amplitudes (ρ_k) are known and deterministic, the autocorrelation matrix is given by

$$\mathbf{R}_{YY} = E_b\tilde{\mathbf{H}}_\rho\tilde{\mathbf{H}}_\rho^H + N_0\mathbf{I}_N + \mathbf{R}_X, \tag{9.13}$$

where $\mathbf{R}_X$ is the autocorrelation matrix of the interference samples in the frequency domain defined as

$$\mathbf{R}_X = \tilde{\mathbf{H}}_\theta^H\mathbf{F}\mathbf{R}_x\mathbf{F}^H\tilde{\mathbf{H}}_\theta, \tag{9.14}$$

where $\mathbf{R}_x$ is the time-domain correlation matrix of the interference, its entries given by

$$r_x(l) = E_x e^{j\frac{2\pi}{N}(m+\alpha)l}. \tag{9.15}$$

Similarly, the cross-correlation vector is given by

$$\mathbf{R}_{YD} = E_b\tilde{\mathbf{H}}_\rho\mathbf{B}. \tag{9.16}$$

For the case of no interference ($\mathbf{R}_X = \mathbf{0}$), the weights are given as

$$\mathbf{W} = \operatorname{diag}\left(\left[\frac{\rho_0 E_b}{\rho_0^2 E_b + N_0}, \frac{\rho_1 E_b}{\rho_1^2 E_b + N_0}, \ldots, \frac{\rho_{N-1} E_b}{\rho_{N-1}^2 E_b + N_0}\right]\right)\mathbf{B}, \tag{9.17}$$

where $\operatorname{diag}(\cdot)$ returns a diagonal matrix from the inputted vector.

When the interference is orthogonal to the subcarriers (except for the m^{th} subcarrier), $\alpha = 0$, recall that **X** will have one non-zero component, at index m. Thus, $\mathbf{R}_X$ will also only have one non-zero value, equal to NE_x at position (m, m). Let $\mathbf{w} = [w(0), \ldots, w(N-1)]$, where $w(l)$ is given by

$$w(l) = \begin{cases} \frac{\rho_l E_b}{\rho_l^2 E_b + N_0}, & l \neq m \\ \frac{\rho_l E_b}{\rho_l^2 E_b + N_0 + N E_x}, & l = m \end{cases}. \tag{9.18}$$

The MMSE weights are then given as

$$\mathbf{W} = \text{diag}\,(\mathbf{w})\,\mathbf{B}. \tag{9.19}$$

It can be seen from (9.19) that when interference is not present on the tone, the weight is the same as for the no-interference case. Note that when $l = m$ and the narrowband interference is strong, then $W_k(l)$ is essentially zero, thus ignoring the subcarrier that is unreliable.

Finally, for the case of a nonorthogonal interferer, the components of the autocorrelation matrix for the interference are given by

$$\mathrm{R}_X(k,l) = \frac{E_x}{N} \frac{2 - 2\cos(2\pi\alpha)}{1 - e^{j\frac{2\pi}{N}(m+\alpha-k)} - e^{-j\frac{2\pi}{N}(m+\alpha-l)} + e^{j\frac{2\pi}{N}(l-k)}},\ k,l = 0,\ldots,N-1. \tag{9.20}$$

To find the weights one could use (9.20) and invert (9.12). However, noticing that $\mathbf{R}_X$ is rank-1, having one dominant eigenvalue, then $\mathbf{R}_X$ can be approximated using the singular value decomposition (SVD) [25] as follows:

$$\begin{aligned} \mathbf{R}_X &= \mathbf{U}\mathbf{S}\mathbf{V}^H \\ &\approx \lambda \mathbf{u}\mathbf{v}^H, \end{aligned} \tag{9.21}$$

where $\lambda = N E_x$ is the non-zero eigenvalue of $\mathbf{R}_X$, $\mathbf{u}$ is the first column of $\mathbf{U}$, and $\mathbf{v}$ is the first column of $\mathbf{V}$. Then using the Sherman–Morrison formula [25], the MMSE combiner weights are derived to be

$$\mathbf{W} = \left(\mathbf{A} - \frac{\lambda \mathbf{A}\mathbf{u}\mathbf{v}^H\mathbf{A}}{1 + \lambda \mathbf{v}^H\mathbf{A}\mathbf{u}} \right) E_b \tilde{\mathbf{H}}_\rho \mathbf{B}, \tag{9.22}$$

where $\mathbf{A} = \text{diag}\left(\left[\frac{1}{\rho_0^2 E_b + N_0}, \frac{1}{\rho_1^2 E_b + N_0}, \ldots, \frac{1}{\rho_{N-1}^2 E_b + N_0} \right] \right)$.

Finally, the estimates of the transmitted data symbols are given by

$$\hat{\mathbf{D}} = \mathbf{W}^H \mathbf{Y}. \tag{9.23}$$

Note that a consequence of MMSE combining in frequency-selective channels is that there is a loss of orthogonality among the data symbols,

$$\hat{\mathbf{D}} = \mathbf{D} + \left(\mathbf{W}^H \tilde{\mathbf{H}}_\rho \mathbf{B} - \mathbf{I}_N \right) \mathbf{D} + \mathbf{W}^H \tilde{\mathbf{H}}_\theta^H \left(\mathbf{X} + \mathbf{N} \right). \tag{9.24}$$

On the other hand, when the channel is AWGN or flat fading, equal gain combining (i.e., $\mathbf{W} = \mathbf{B}$) can be utilized to preserve orthogonality, that is

$$\hat{\mathbf{D}} = \mathbf{D} + \mathbf{W}^H \tilde{\mathbf{H}}_\theta^H \left(\mathbf{X} + \mathbf{N} \right). \tag{9.25}$$

9.3.1.2 OFDM

Unlike MC-CDMA, OFDM does not provide frequency diversity since the code matrix in Fig. 9.5 is set to the identity matrix. The prediction-error filter (PEF) is considered for this system as a means for removing the interference in the time domain, thereby avoiding the spectral leakage that occurs after demodulation (see block diagram given in Fig. 9.6). The PEF is a well-studied structure that uses the correlation between past samples to form an estimate of the current sample [40]. The PEF has the property that it removes the correlation between samples, thereby whitening the spectrum.

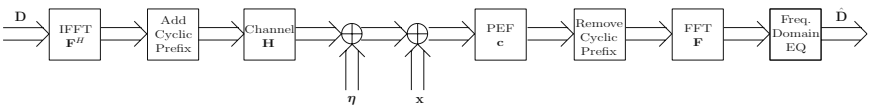

Fig. 9.6 Block diagram of uncoded OFDM with the PEF

This technique has been used to remove narrowband interference in many applications, such as spread-spectrum systems when the processing gain does not provide enough immunity to the interference [49, 53]. A block diagram of the PEF is shown in Fig. 9.7. It is simply a transversal filter with M taps. The decorrelation delay (Δ) ensures that the current sample is decorrelated from the samples in the filter when calculating the error term.

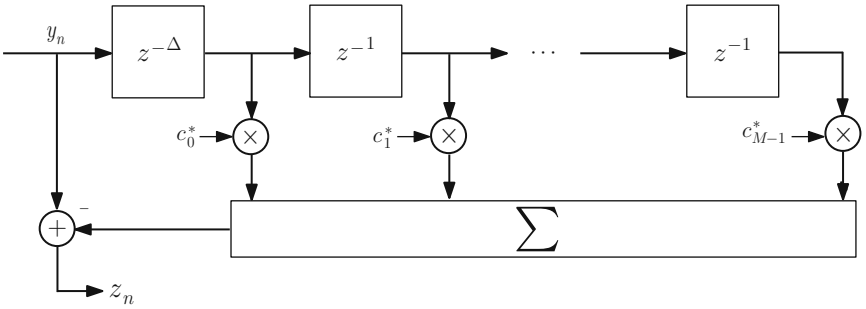

Fig. 9.7 Block diagram of the prediction-error filter (PEF)

The output of the PEF, z_n, is defined as the subtraction of the estimate of the interference from the current input sample,

$$z_n = y_n - \sum_{l=0}^{M-1} c_l^* y_{n-\Delta-l}, \tag{9.26}$$

where c_l are the weights of the predictor and $(\cdot)^*$ represents complex conjugation. The optimal weights under the minimum mean-squared error (MMSE) criterion are

found using the orthogonality principle and the method of undetermined coefficients [61]. The weights are given by

$$c_l = Ke^{-j\frac{2\pi}{N}(m+\alpha)(l+\Delta)}, \quad l = 0, \ldots, M-1, \tag{9.27}$$

where K is given by

$$K = \frac{E_x}{E_b + N_0 + ME_x}. \tag{9.28}$$

For the scenario of interest in this chapter, the interference power is much larger than both the signal power and the noise power. Therefore, the SIR and the noise to interference (NIR) can be assumed to be very small (i.e., SIR $\ll 0$ dB, NIR $\ll 0$ dB [31]) allowing the coefficient, K, to be approximated as $K \approx \frac{1}{M}$.

This filter is easily implemented adaptively using the least mean square (LMS) algorithm. The convergence properties are well described [5, 42]. Note also that z_n is the error term for the adaptive structure, indicating that no training symbols are required when calculating the error term.

The PEF is implemented before the removal of the cyclic prefix. Let the one-step predictor weights be defined as $\mathbf{c} = \left[1, -c_0^*, \ldots, -c_{M-1}^*\right]$ and the convolution of the filter and channel be defined as $\mathbf{a} = \mathbf{c} * \mathbf{h}$. It is assumed that the overall length of $\mathbf{a}$ is less than the length of the cyclic prefix (i.e., $L + M - 1 \leq G$) to ensure that there is no ISI or ICI. Therefore, the effective channel matrix, $\mathbf{A}$, is circulant. Then, the filtered signal in the frequency domain can be written as

$$\begin{aligned} \mathbf{Z}' &= \mathbf{FAF}^H\mathbf{D} + \mathbf{FC}_{\text{noise}}\left(\mathbf{x}_{\text{cp}} + \boldsymbol{\eta}_{\text{cp}}\right) \\ &= \tilde{\mathbf{A}}\mathbf{D} + \mathbf{FC}_{\text{noise}}\left(\mathbf{x}_{\text{cp}} + \boldsymbol{\eta}_{\text{cp}}\right), \end{aligned} \tag{9.29}$$

where $\tilde{\mathbf{A}}$ is the diagonal matrix of the eigenvalues of $\mathbf{A}$, $\mathbf{x}_{\text{cp}}$ and $\boldsymbol{\eta}_{\text{cp}}$ are vectors of interference and noise samples (length $N + G$), respectively that are not cyclically extended, and $\mathbf{C}_{\text{noise}}$ is the $N \times (N+G)$ filtering matrix for the noise and interference that is defined as

$$\mathbf{C}_{\text{noise}} = \left[\mathbf{0}_{N,G-M}\ \text{Toeplitz}\left(\left[c_{M-1}^*, \mathbf{0}_{1,N-1}\right]^T \left[\mathbf{c}^*, \mathbf{0}_{1,N-1}\right]\right)\right], \tag{9.30}$$

where $\mathbf{0}_{i,j}$ is the $i \times j$ zero matrix. The Toeplitz operator, Toeplitz$(column, row)$, generates a Toeplitz matrix from a column vector and a row vector. Note that $\tilde{\mathbf{A}}$ in (9.32) can also be defined as

$$\tilde{\mathbf{A}} = \tilde{\mathbf{H}}\tilde{\mathbf{C}}, \tag{9.31}$$

where $\tilde{\mathbf{C}} = \sqrt{N}\mathbf{F}\left[\mathbf{c}^*\ \mathbf{0}_{1,N-(M+1)}\right]^T$. This vector is the sampled frequency response of the notch filter, with the notch located on the tone closest to the interference.

For coherent demodulation, the phase of the effective channel matrix $\tilde{\mathbf{A}}$ must be removed; therefore, similar to (9.5) and (9.6), let $\tilde{\mathbf{A}} = \tilde{\mathbf{A}}_\theta\tilde{\mathbf{A}}_\rho$, where $\tilde{\mathbf{A}}_\rho = |\tilde{\mathbf{A}}|$ and $\tilde{\mathbf{A}}_\theta = e^{\angle\tilde{\mathbf{A}}}$. Thus for coherent demodulation,

$$\mathbf{Z} = \tilde{\mathbf{A}}_\theta^H \mathbf{Z}' = \tilde{\mathbf{A}}_\rho \mathbf{D} + \tilde{\mathbf{A}}_\theta^H \mathbf{F} \mathbf{C}_{\text{noise}} \left(\mathbf{x}_{\text{cp}} + \boldsymbol{\eta}_{\text{cp}} \right). \tag{9.32}$$

Note that the diagonal elements of $\tilde{\mathbf{A}}_\rho$ are not necessarily distributed as Rayleigh random variables due to the PEF.

Let the uncanceled interference and noise be grouped into one general noise term

$$\tilde{\mathbf{N}} = \tilde{\mathbf{A}}_\theta^H \mathbf{F} \mathbf{C}_{\text{noise}} \left(\mathbf{x}_{\text{cp}} + \boldsymbol{\eta}_{\text{cp}} \right). \tag{9.33}$$

It is clear from (9.33) that the noise samples, $\tilde{N}_k$, are correlated due to the PEF matrix, $\mathbf{C}_{\text{noise}}$. It is also noted that the noise samples $\tilde{N}_k$ are assumed to be Gaussian random variables. As stated in [31], this system is difficult to analyze when the noise samples are not strictly independent, however, due to the fact that the noise power in the main tap (equal to unity) is much larger than in the remaining taps (approximately $\frac{1}{M}$ for the scenario of interest in this chapter), it is reasonable to assume that the noise samples are independent. Therefore, let $\sigma_{\tilde{N}}^{2(k)}$ be the variance of the noise on tone k, given by

$$\begin{aligned} \sigma_{\tilde{N}}^2(k) &= E\left[\tilde{N}_k \tilde{N}_k^H \right] \\ &= \left[\tilde{\mathbf{A}}_\theta^H \mathbf{F} \mathbf{C}_{\text{noise}} \left(\mathbf{R}_x + \frac{N_0}{2} \mathbf{I}_N \right) \mathbf{C}_{\text{noise}}^H \mathbf{F}^H \tilde{\mathbf{A}}_\theta \right]_{kk}. \end{aligned} \tag{9.34}$$

Note that the variances given in (9.34) are scaled according to the notch filter that is used to suppress the interference.

One-tap equalization is performed instead of MMSE combining as is done for MC-CDMA. Thus the estimates of the transmitted data symbols are given by

$$\hat{\mathbf{D}} = \mathbf{Z} / \tilde{\mathbf{A}}_\rho. \tag{9.35}$$

An analytic expression for the BER of this OFDM system given knowledge of the channel amplitudes is simply the average of the per-tone BER, given by

$$P_e = \frac{1}{N} \sum_{k=0}^{N-1} Q\left(\sqrt{\frac{|\tilde{A}_\rho(k)|^2 E_b}{\sigma_{\tilde{N}}^2(k)}} \right). \tag{9.36}$$

The analytical results of (9.36) are seen in Fig. 9.8 along with the simulation results for SIR $= -20$ dB and $N = 64$, $G = 16$, $L = 5$, and $M = 12$. The simulation and theoretical results agree quite well, validating the assumption of independent noise samples. Also note that an error floor arises, because the OFDM system is limited by its worst set of tones. In this case, these tones are the ones located around the notch generated by the PEF. This suggests the need for forward error correction coding. The addition of a convolutional code can reduce the BER from 10^{-2} to 10^{-5}. Note that without the use of the PEF, the BER is so poor that forward error correction coding cannot be effectively employed.

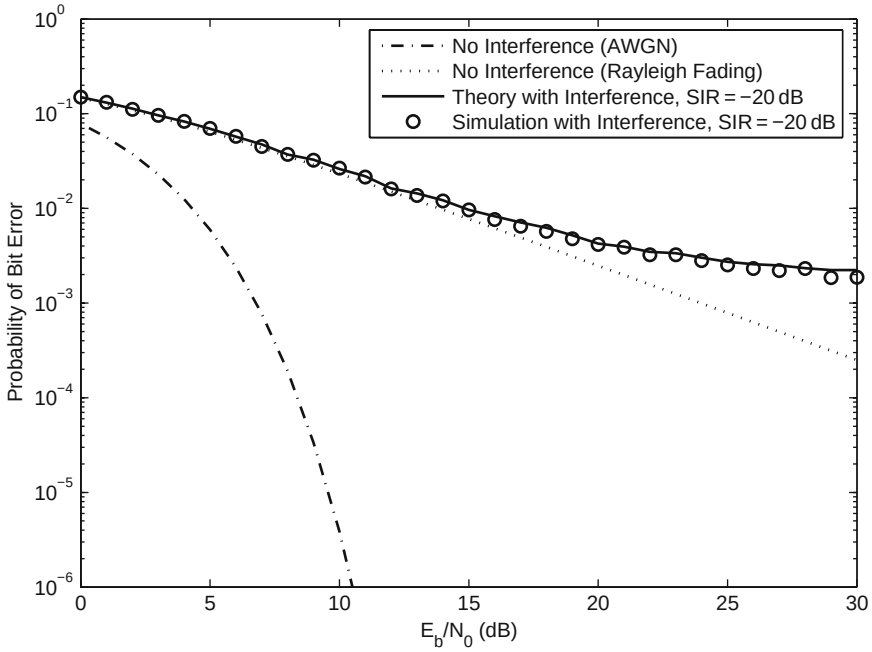

Fig. 9.8 Uncoded BER results for theoretical and simulated OFDM with the prediction-error filter (PEF). Also plotted are the theoretical BER curves for AWGN and Rayleigh fading. Parameters: $N = 64$, $G = 16$, $L = 5$, $M = 12$, SIR $= -20$ dB

9.3.1.3 Results

A comparison of the two techniques described previously is compared in an uncoded scenario in Fig. 9.9. For reference, the theoretical BER curves for both AWGN and Rayleigh fading are provided. Each system is simulated for the cases (i) no interference and (ii) one nonorthogonal interferer. The plot for MC-CDMA in no interference indicates that frequency diversity provides a benefit in a frequency-selective channel. The performance of MC-CDMA with a single nonorthogonal interferer is very close to the case of no interference. In this case, the combiner utilizes the statistics of the channel and interference to successfully recombine the transmitted signal. The deviation from the case of no interference is very small.

The PEF used with OFDM assumes knowledge of the MMSE weights given in (9.27). In the presence of no interference the performance of the system reduces to that of Rayleigh fading, as is expected. When interference is present, the case of a nonorthogonal interference approximates the case of Rayleigh fading at low E_b/N_0 values; however at high E_b/N_0 values, an error floor arises. This is due to the notch filter that removes a few tones when mitigating the interference.

For both MC-CDMA and OFDM with PEF, the interference must be estimated in order to be implemented in a real-world communication system. As mentioned earlier, the PEF is easily implemented using the low-complexity LMS algorithm without training symbols. This allows the interference to be adaptively estimated

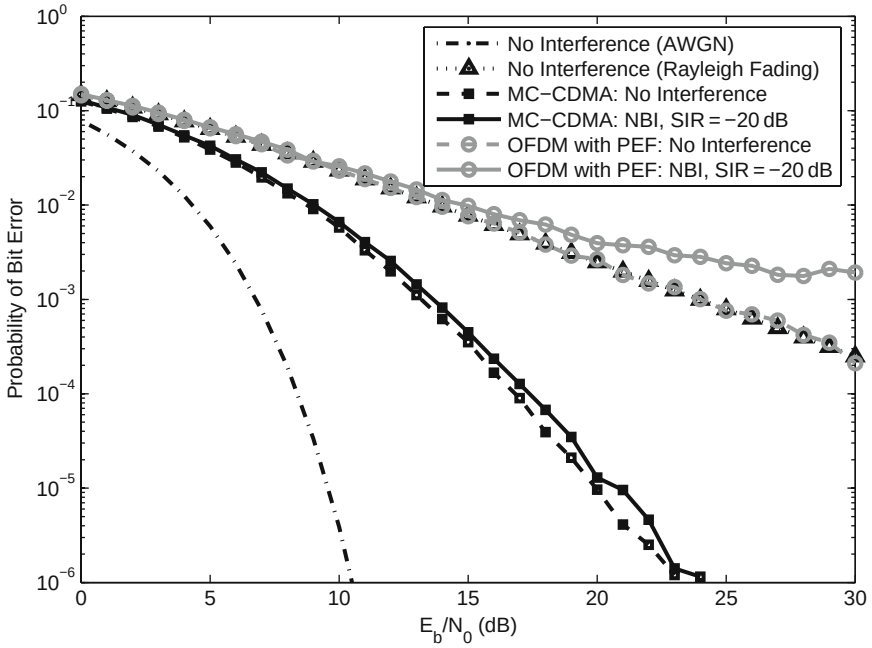

Fig. 9.9 Uncoded BER results for MC-CDMA and OFDM with the prediction-error filter (PEF) for the cases of (i) no interference and (ii) one nonorthogonal interferer. Also plotted are the theoretical BER curves for AWGN and Rayleigh fading. Parameters: $N = 64$, $G = 16$, $L = 5$, $M = 12$, SIR $= -20$ dB

and removed. In the case of MC-CDMA, the correlation matrix of the interference is required when determining the MMSE combiner weights. This can be accomplished using training symbols to provide an estimate for the received signal correlation matrix.

9.3.2 Interference Mitigation in Coded Multicarrier Systems

In this section, the impact of applying forward error correction to the uncoded systems analyzed above is evaluated. Block diagrams for coded MC-CDMA and coded OFDM with PEF are depicted in Figs. 9.10 and 9.11, respectively. A convolutional code of rate $1/2$, constraint length equal to 7 with generating polynomials $(133, 171)_8$ is used. One codeword spans 50 MC-CDMA/OFDM symbols. At the receiver the Viterbi [39] decoder is used to decode the codeword utilizing soft decisions. Note that a block interleaver is used with OFDM to provide frequency diversity. An interleaver can also be used with MC-CDMA when the data are spread over a subset of the subcarriers.

The soft decisions inputted into the Viterbi decoder encourage the use of erasures when reliable log-likelihood ratios (LLRs) are unavailable. In OFDM, erasures are

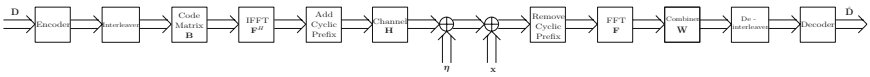

Fig. 9.10 Block diagram for coded MC-CDMA

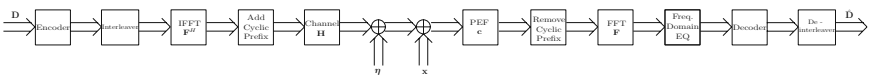

Fig. 9.11 Block diagram for coded OFDM with the PEF

only effective when the interference is weak [4]. However, when the interference is strong, the spectral leakage of interference power causes a large number of tones to be corrupted. Insertion of erasures ends up compromising the code's error correction capability. The use of the PEF can be considered as a form of erasure insertion, whereby the erasures are localized around the interference by the notch that is placed in the frequency spectrum of the received signal. The code is then tasked with correcting any erasures caused by the channel or interference. The full erasures are inserted after the PEF using the Bayesian erasure formula described in [6].

The LLR values [15] that are inputted into the Viterbi decoder for MC-CDMA with BPSK modulation are given as

$$\Lambda_{\text{MC-CDMA}}(D_k|Y_k) = \frac{2\Re\{Y_k\}}{\sigma^2}, \tag{9.37}$$

where $\Re\{\cdot\}$ is the real operator and σ^2 is the variance of the ICI, noise, and interference as defined in (9.24). Assuming these vectors are composed of independent Gaussian random variables, σ^2 is given as follows:

$$\sigma^2 = \text{diag}\left[E_b \left(\mathbf{W}^H \tilde{\mathbf{H}}_\rho \mathbf{B} - \mathbf{I}\right)\left(\mathbf{W}^H \tilde{\mathbf{H}}_\rho \mathbf{B} - \mathbf{I}\right)^H + \tfrac{N_0}{2}\mathbf{W}\mathbf{W}^H + \mathbf{W}^H \tilde{\mathbf{H}}_\theta^H \mathbf{F}\mathbf{R}_x \mathbf{F}^H \tilde{\mathbf{H}}_\theta \mathbf{W} \right]. \tag{9.38}$$

Similarly, for OFDM

$$\Lambda_{\text{OFDM}}(D_k|Z_k) = \frac{2\Re\{Z_k\}}{\sigma^2}, \tag{9.39}$$

where σ^2 is given as

$$\sigma^2 = \frac{\text{diag}\left[\tilde{\mathbf{A}}_\theta^H \mathbf{F}\mathbf{C}_{\text{noise}}\left(\mathbf{R}_x + \frac{N_0}{2}\mathbf{I}_N\right)\mathbf{C}_{\text{noise}}^H \mathbf{F}^H \tilde{\mathbf{A}}_\theta\right]}{\text{diag}\left[\tilde{\mathbf{A}}_\rho \tilde{\mathbf{A}}_\rho^H\right]}. \tag{9.40}$$

9.3.2.1 Results

Figure 9.12 demonstrates the results for the coded simulation of MC-CDMA and OFDM with the PEF for the cases of (i) no interference and (ii) one nonorthogonal interferer, for $N = 64$, $G = 16$, $L = 5$, $M = 12$, SIR $= -20$ dB. Also plotted are the theoretical BER curves for uncoded Rayleigh fading and a BER bound for AWGN. It can be clearly seen that the performance of both systems with interference is very close to the case of no interference. Also note that the performance of OFDM with frequency diversity provided by coding and the PEF as an erasure insertion technique is equivalent to that of coded MC-CDMA for which frequency diversity is obtained through spreading. The coding gain is also apparent when comparing the coded results with Fig. 9.9.

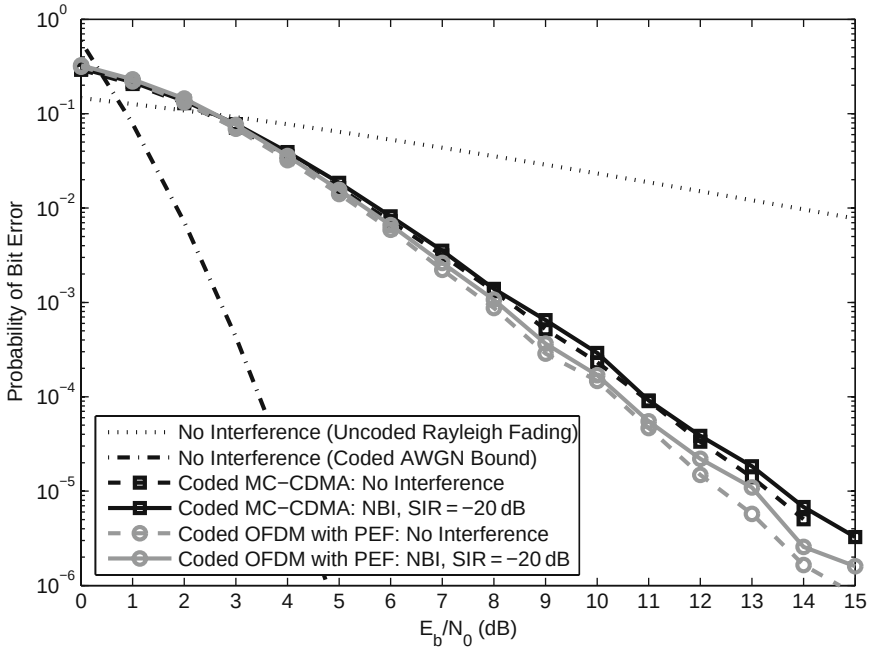

Fig. 9.12 Coded BER results for MC-CDMA and OFDM with the prediction-error filter (PEF) for the cases of (i) no interference and (ii) one nonorthogonal interferer. Also plotted are the theoretical BER curves, uncoded Rayleigh Fading, and a BER bound for AWGN. Parameters: $N = 64$, $G = 16$, $L = 5$, $M = 12$, SIR $= -20$ dB

9.3.3 Doppler Sensitivity of OFDM in Mobile Applications

Mobile systems that employ OFDM may suffer degradations from ISI and ICI in addition to the other forms of interference discussed above. In [50], the Doppler sensitivity of OFDM was investigated for PSK and QAM modulations in the presence

of ICI and the loss in performance due to Doppler spreading was evaluated. Also, in [52], comparisons were made between the Doppler sensitivity of OFDM and filtered multitone (FMT) modulation in frequency-selective time-varying channels.

FMT is an alternate form of multicarrier modulation that has been proposed for very high-rate subscriber lines and for wireless communications. FMT avoids spectral overlap between subcarriers by implementing a noncritical sampling technique that satisfies a perfect reconstruction condition, so that the sampling signals at the receiver are free from ISI as well as ICI. The ISI and ICI in an FMT system is suppressed at the expense of choosing a larger upsampling-factor-to-number-of-subcarriers ratio. Due to the phase and amplitude distortion introduced by the fading channel, not only is the orthogonality among different subcarriers destroyed but also the perfect Nyquist sampling condition of the baseband matched filters is no longer valid. Consequently, ICI as well as ISI will cause distortions to the transmitted signal. The interference caused by the channel frequency selectivity and time variance was quantified by analyzing the demodulated signals at the receiver under different fading channel conditions. It was shown [52] analytically that quasi-static frequency flat fading channels do not introduce ICI or ISI to a multicarrier system, while frequency-selective channels introduce both ISI and ICI in an FMT system. The resulting carrier-to-interference (C/I) ratio obtained under different channel conditions was shown to provide a trade-off between spectral efficiency and system performance degradation. Also it was shown [52] that OFDM outperforms FMT in a static or slowly fading and low frequency-selective channel but is inferior to FMT modulation in highly frequency-selective and time-varying fading environments.

This work was extended in [51] to consider a per-channel-equalized FMT architecture. It is shown that with a sufficient number of equalizer coefficients it is possible to mitigate the ISI, but the ICI remains. A closed-form analytical expression for the C/I ratio and its upper bound is derived and the trade-offs in spectral efficiency and system performance are further quantified.

9.4 Interference Suppression in Broadcast MIMO Systems

In this section, we consider multiple-input, multiple-output (MIMO) wireless communication systems that employ multiple-transmit and multiple-receive antennas to increase the data rate and achieve signal diversity in fading multipath channels. The performance of MIMO systems is degraded by two types of interference. One is intersymbol interference due to channel multipath dispersion. The other is crosstalk or interchannel interference due to the simultaneous transmissions from the multiple-transmit antennas. The focus of this section is on equalization and detection algorithms for mitigating these two types of interference. In particular, we consider a point-to-multipoint (broadcast) MIMO transmission system in which the channel characteristics are assumed to be known at the transmitter, so that interference mitigation is performed at the transmitter.

Let us consider a point-to-multipoint MIMO system which transmits data simultaneously to multiple users that are geographically distributed. The transmitter is assumed to employ N_T antennas to transmit data to K receivers, where $N_T \geq K$. Each user is assumed to have a receiver with one or more receiving antennas. This scenario applies, for example, to the downlink of a wireless local area network. The distinguishing feature of the MIMO broadcast system is that the receivers, which are geographically separated, do not employ any coordination in processing the received signals.

In a MIMO broadcast system, there are two possible approaches for dealing with the multiple-access interference (MAI) resulting from the simultaneous transmission to multiple users. One approach is to have each receiver employ interference mitigation in the recovery of its desired signal. In most cases, this approach is impractical because the users lack the processing capability and are constrained by the limited energy resources inherent in the use of battery power. The alternative approach is to employ interference mitigation at the transmitter, which possess significantly more processing capability and energy resources.

To mitigate the MAI at the transmitter, the transmitter must know the channel characteristics, typically the channel impulse response. This channel state information (CSI) may be obtained from channel measurements performed at each of the receivers by means of received pilot signals sent by the transmitter. Then, the CSI must be sent to the transmitter. In such a scenario, the channel time variations must be relatively slow so that a reliable estimate of the channel characteristics is available at the transmitter. In some systems, the uplink and downlink channels are identical, e.g., the same frequency band is employed for both the uplink and the downlink, but separate time slots are used for transmission. This transmission mode is called time-division duplex (TDD). In TDD systems, the pilot signals for channel measurement may be sent by each of the users in the uplink. In our treatment below, we assume that the CSI at the transmitter is perfect.

The suppression of MAI by means of transmitter processing is usually called signal precoding or signal preprocessing. Signal precoding at the transmitter may take one of several forms, depending on the criterion or the method used to perform the precoding. The simplest precoding methods are linear and are based on either the zero-forcing (ZF) criterion or the MSE criterion. On the other hand, there are nonlinear signal precoding methods that result in better system performance. First, we treat linear precoding and, then, we describe nonlinear precoding methods and compare their performance.

9.4.1 Linear Precoding of the Transmitted Signals

In this section, for mathematical convenience, we assume that each user has a single antenna and the number of receivers (users) is $K \leq N_T$. It is also convenient to assume that the channel is nondispersive. The communication system configuration is shown in Fig. 9.13, where the precoding matrix is denoted as $\mathbf{A}_T$. Hence, the received signal vector is

$$\mathbf{y} = \mathbf{H}\mathbf{A}_T\mathbf{s} + \boldsymbol{\eta}, \tag{9.41}$$

where $\mathbf{H}$ is an $K \times N_T$ matrix, $\mathbf{A}_T$ is an $N_T \times K$ precoding matrix, $\mathbf{s}$ is a $K \times 1$ data vector, and $\boldsymbol{\eta}$ is a $K \times 1$ Gaussian noise vector. The matrix that eliminates the MAI at each receiver is generally given by the Moore–Penrose pseudo-inverse

$$\mathbf{H}^{+} = \mathbf{H}^{H}(\mathbf{H}\mathbf{H}^{H})^{-1}. \tag{9.42}$$

Hence, the precoding matrix is

$$\mathbf{A}_T = \gamma\mathbf{H}^{+}, \tag{9.43}$$

where γ is a scale factor that is selected to satisfy the total transmitted power allocation, i.e., $\| \mathbf{A}_T\mathbf{s} \|^2 = P$. Thus, the precoding matrix in (9.43) allows the individual users to recover their desired symbols without any interference from the signals transmitted to the other users. We also observe that in the special case where $K = N_T$, $\mathbf{A}_T = \gamma\mathbf{H}^{-1}$, so that the precoding matrix is proportional to the inverse channel matrix. This constitutes a zero-forcing equalizer implemented at the transmitter.

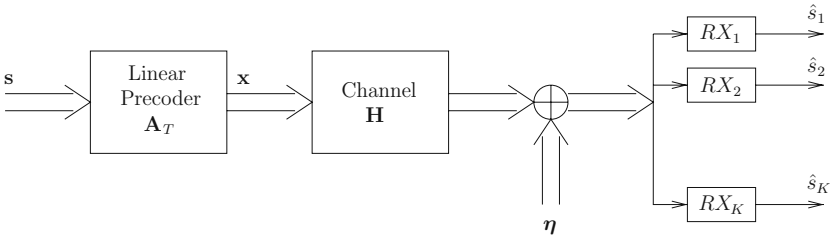

Fig. 9.13 Model of MIMO broadcast system employing linear precoding

Figure 9.14 illustrates the error rate performance of the zero-forcing precoder obtained via Monte Carlo simulation for $K = N_T = 4$, 6, and 10 and QPSK modulation. The channel matrix elements are realizations of complex-valued i.i.d. zero-mean Gaussian random variables with unit variance. We observe that the error rate increases with an increase in the number of users. We attribute this deterioration in performance to the ill-conditioning of the channel matrix $\mathbf{H}$. This is the major drawback with the zero-forcing precoder.

If we relax the condition that the interference be zero at all the receivers, the performance degradation can be reduced. This can be accomplished by using the linear MSE criterion in the design of the precoding matrix $\mathbf{A}_T$. Thus, we select $\mathbf{A}_T$ to minimize the cost function

$$J(\mathbf{A}_T, \gamma) = \arg\min_{\gamma, \mathbf{A}_T} E \left\| \frac{1}{\gamma}(\mathbf{H}\mathbf{A}_T\mathbf{s} + \boldsymbol{\eta}) - \mathbf{s} \right\|^2, \tag{9.44}$$

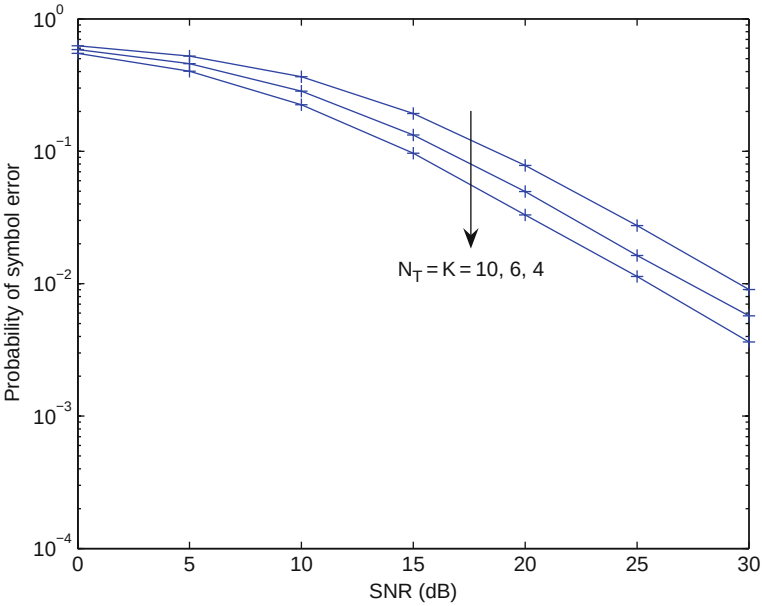

Fig. 9.14 Performance of ZF linear precoding with $N_T = K = 4, 6, 10$

subject to the transmitted power allocation $\|\mathbf{A}_T\mathbf{s}\|^2 = P$ and where the expectation in (9.44) is taken over the noise and signal statistics. The solution to the MSE criterion is the precoding matrix

$$\mathbf{A}_T = \gamma \mathbf{H}^H (\mathbf{H}\mathbf{H}^H + \beta \mathbf{I})^{-1}, \tag{9.45}$$

where γ is the scale factor that is selected to satisfy the power allocation and β is defined as a loading factor, which when selected as $\beta = K/P$ maximizes the signal-to-interference-plus-noise ratio (SINR) at the receiver [38].

The error rate performance of the MMSE linear precoder obtained by Monte Carlo simulation in a frequency-nonselective Rayleigh fading channel is illustrated in Fig. 9.15 for $K = N_T = 4, 6$, and 10. We observe that the error rate performance improves slightly as the number of users K increases and that it exceeds the performance of the zero-forcing precoder.

9.4.2 Nonlinear Precoding of the Transmitted Signals: The QR Decomposition

When the transmitter knows the interference caused on other users by the transmission of a signal to any particular user, the transmitter can design signals for each of the other users to cancel the interference. The major problem with such an

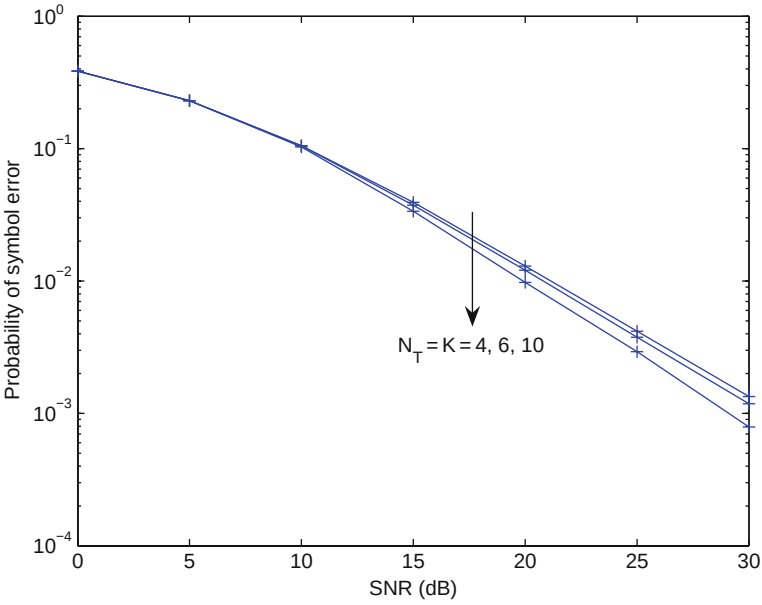

Fig. 9.15 Performance of MMSE linear precoding with $N_T = K = 4, 6, 10$

approach is to perform the interference cancellation without increasing the transmitter power. This same problem is encountered in decision-feedback channel equalization of a single user, where the feedback filter of the DFE is implemented at the transmitter. In that case, when the difference between the desired transmitted symbol and the ISI exceeds the range of the desired transmitted symbol, the difference is reduced by subtracting an integer multiple of $2M$ for M-ary PAM, where $[-M, M)$ is the range of the desired transmitted symbol. This same nonlinear precoding method called Tomlinson-Harashima precoding [24, 47] can be applied to the cancellation of the MAI in a MIMO broadcast communication system [17, 18, 56].

Figure 9.16 illustrates the precoding operations for the MIMO multiuser system. The channel impulse response between the ith transmit antenna and the receive antenna of the kth user is given by

$$h_{ki}(t) = \sum_{l=0}^{L-1} h_{ki}^{(l)} \delta(t - lT), \tag{9.46}$$

where L is the number of multipath components in the channel response, T is the symbol duration, and $h_{ki}^{(l)}$ is the complex-valued channel coefficient for the lth path. The channel coefficients $\{h_{ki}^{(l)}\}$ are known at the transmitter and are realizations of i.i.d. zero-mean, circularly symmetric complex Gaussian random variables with variance

$$E\left[|h_{ki}^{(l)}|^2\right] = \frac{1}{L} \ \forall k, i \text{ and } l. \tag{9.47}$$

It is convenient to arrange these channel coefficients for the lth path in a $K \times N_T$ matrix $\mathbf{H}^{(l)}$, where $[\mathbf{H}^{(l)}]_{ki} = h_{ki}^{(l)},\ i = 1, 2, \ldots, N_T,\ k = 1, 2, \ldots, K$.

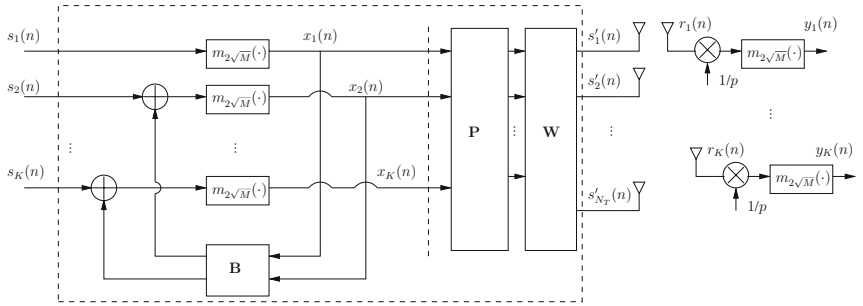

Fig. 9.16 Tomlinson-Harashima precoding applied to MIMO system

The MAI cancellation is facilitated by use of the QR decomposition of the channel matrix $\mathbf{H}^{(0)}$. Thus, we express $[\mathbf{H}^{(0)}]^H$ as

$$[\mathbf{H}^{(0)}]^H = \mathbf{QR}, \tag{9.48}$$

where $\mathbf{Q}$ is an $N_T \times K$ matrix, such that $\mathbf{QQ}^H = \mathbf{I}$, and $\mathbf{R}$ is a $K \times K$ upper triangular matrix with diagonal elements $\{r_{ii}\}$. Based on this decomposition of $[\mathbf{H}^{(0)}]^H$, the signal to be transmitted is precoded with the matrix transformation

$$\mathbf{W} = \mathbf{QA}, \tag{9.49}$$

where $\mathbf{A}$ is a $K \times K$ diagonal matrix with diagonal elements $1/r_{ii}\ ,\ i = 1, 2, \ldots, K$. The $\{r_{ii}\}$ are real and positive [48]. The matrix $\mathbf{P} = p\mathbf{I}$ is a diagonal $K \times K$ matrix that is used simply for scaling the power of the transmitted signal and results in equal SNR for all users. Therefore, we have an effective channel matrix of the form

$$\begin{aligned} \mathbf{H}^{(0)}\mathbf{WP} &= [\mathbf{QR}]^H\mathbf{QAP} \\ &= p\mathbf{R}^H\mathbf{A}. \end{aligned} \tag{9.50}$$

We note that $\mathbf{R}^H\mathbf{A}$ is a $K \times K$ lower triangular matrix with unit diagonal elements. As a result, user k sees multiple-access interference from users $1, 2, \ldots, k-1$. We also note that the effective channel matrix $\mathbf{H}^{(0)}\mathbf{W} = \mathbf{R}^H\mathbf{A}$ will have full rank K, provided that $N_T \geq K$.

By reducing this channel matrix to a lower triangular matrix, we can now subtract the interference at the transmitter that each user would normally observe at their respective receivers. Thus, when the channel adds the same interference to the transmitted signal, the received signal at each receiver would be free of interference.

Taking advantage of the lower triangular matrix structure, successive interference cancellation is performed with the feedback filter defined by the matrix

$$\mathbf{B} = [\mathbf{I} - \mathbf{H}^{(0)}\mathbf{W}, -\mathbf{H}^{(1)}\mathbf{W}\ ,\ -\mathbf{H}^{(2)}\mathbf{W}, \ldots, -\mathbf{H}^{(L-1)}\mathbf{W}], \tag{9.51}$$

where the matrix $(\mathbf{I}-\mathbf{H}^{(0)}\mathbf{W})$ is used to cancel the interference due to the other users that arises in the current symbol interval, and the terms $-\mathbf{H}^{(1)}\mathbf{W}$, $-\mathbf{H}^{(2)}\mathbf{W}$, $\ldots$, $-\mathbf{H}^{(L-1)}\mathbf{W}$ are used to cancel the interference due to previous symbols.

To ensure that the subtraction of the interference terms do not result in an increase of transmitter power, we use the modulo operator, as in Tomlinson-Harashima precoding, to limit the range of the signal to the boundaries of the signal constellation. Thus, the output of the modulo operators for the nth symbol vector, as shown in Fig. 9.16 (for square QAM constellations) is

$$\begin{aligned}\mathbf{x}_n &= \mathrm{mod}_{2\sqrt{M}}[\mathbf{s}_n + \mathbf{B}\hat{\mathbf{x}}_n] \\ &= \mathbf{s}_n + \mathbf{B}\hat{\mathbf{x}}_n - 2\sqrt{M}\mathbf{z}_n,\end{aligned} \tag{9.52}$$

where the modulo operation is performed on each real and imaginary components of the vector $[\mathbf{s}_n + \mathbf{B}\hat{\mathbf{x}}_n]$, $\mathbf{x}_n$ is the $K \times 1$ vector at the output of the modulo operator, $\mathbf{s}_n$ is the $K \times 1$ data vector, $\hat{\mathbf{x}}_n$ is defined as

$$\hat{\mathbf{x}}_n = [\mathbf{x}_n^T\ ,\ \mathbf{x}_{n-1}^T\ ,\ \mathbf{x}_{n-2}^T\ , \ldots,\ \mathbf{x}_{n-(L-1)}^T]^T, \tag{9.53}$$

and $\mathbf{z}_n$ is a $K \times 1$ vector with complex-valued components that take on integer values, determined by the constraint that the real and imaginary components of $\mathbf{x}_n$ fall in the range of $[-\sqrt{M}, \sqrt{M})$. Therefore, the transmitted signal vector is expressed as

$$\begin{aligned}\mathbf{s}_n' &= \mathbf{W}\mathbf{P}\mathbf{x}_n \\ &= p\mathbf{W}\mathbf{x}_n\end{aligned} \tag{9.54}$$

and the received signal vector is

$$\mathbf{r}_n = p\sum_{i=0}^{L-1}\mathbf{H}^{(i)}\mathbf{W}\mathbf{x}_{n-i} + \boldsymbol{\eta}_n, \tag{9.55}$$

and, hence,

$$\begin{aligned}\mathbf{P}^{-1}\mathbf{r}_n = \mathbf{x}_n &+ (\mathbf{H}^{(0)}\mathbf{W} - \mathbf{I})\mathbf{x}_n \\ &+ \sum_{i=1}^{L-1}\mathbf{H}^{(i)}\mathbf{W}\mathbf{x}_{n-i} + \boldsymbol{\eta}_n'.\end{aligned} \tag{9.56}$$

By substituting for $\mathbf{B}$ and $\mathbf{x}_n$ in (9.56), it follows that

$$\mathbf{P}^{-1}\mathbf{r}_n = \mathbf{s}_n + \boldsymbol{\eta}_n' - 2\sqrt{M}\mathbf{z}_n. \tag{9.57}$$

Consequently, the MAI and ISI are cancelled perfectly, resulting in the test statistics for the nth symbol vector as follows:

$$\mathbf{y}_n = \mathrm{mod}_{2\sqrt{M}}\left[\frac{1}{p}\mathbf{r}_n\right]. \tag{9.58}$$

9.4.2.1 Optimum Ordering of the Decentralized Receivers

The ordering of the K decentralized receivers affects the construction of the $K \times N_T$ channel matrix $\mathbf{H}^{(0)}$. There are $K!$ possible column permutations of $[\mathbf{H}^{(0)}]^H$ and, hence, there is one QR decomposition associated with each permutation. In turn, there are $K!$ transformation matrices $\mathbf{W} = \mathbf{QA}$, each of which requires a different transmit power. In order to minimize the total transmit power, it is necessary to search over all the column permutations. Such an exhaustive search procedure is computationally time-consuming, except for a small number of users. A method for simplifying the search for the optimum ordering is described in [19].

The error rate performance of the QR decomposition method described above has been evaluated in [1, 2]. Figure 9.17 illustrates the symbol error probability as a function of the SNR (total transmitted signal power over all antennas divided by N_0) for QPSK modulation, $L = 1, 2$ and $N_T = K = 2$. The Monte Carlo simulation results are also illustrated. The simulation results are obtained by transmitting 1,000 data symbols over each of 10,000 channel realizations.

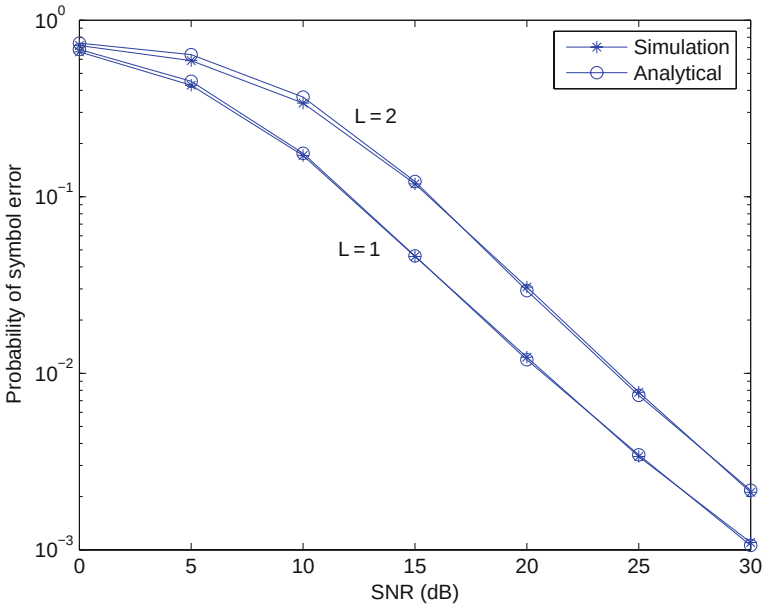

Fig. 9.17 Performance of optimal-ordered QR decomposition with $N_T = K = 2$ and $L = 1, 2$

Figure 9.18 shows analytical results of the symbol error rate performance for QPSK with $L = 1$ (flat fading), $K = 2$, and $N_T = 2, 3, 4$. We observe that the system performance improves with an increase in the number of transmit antennas, which reflects the benefit of spatial diversity.

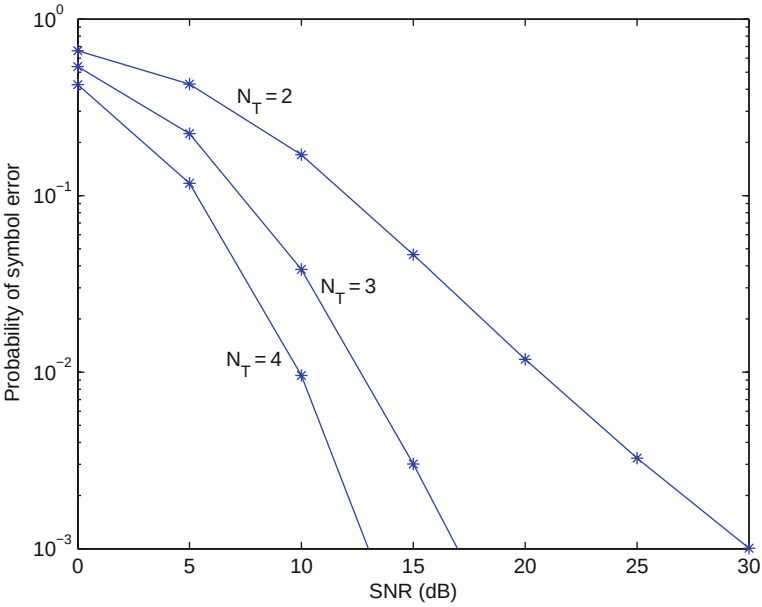

Fig. 9.18 Performance of optimal-ordered QR decomposition with $K = 2, L = 1$, and $N_T = 2, 3, 4$

Figure 9.19 shows simulation results comparing the error rate performance of the linear zero-forcing (ZF) and minimum MSE (MMSE) precoding methods with the QR decomposition method for QPSK modulation with $L = 1$ and $K = N_T = 4$. We observe that the performance of the QR decomposition method is better than that of the linear precoders at high SNR, but poorer at low SNR. It should be noted that the improvement in performance of the QR decomposition method at high SNR is obtained at a significantly higher computational complexity compared with the linear precoders.

9.4.3 Vector Precoding

Hochwald et al. [26] have described and evaluated the performance of a vector precoding method in which the data vector $\mathbf{s}$ to be transmitted to the K users is modified by the addition of a precoding vector with integer elements as illustrated in Fig. 9.20. That is, the modified signal vector is defined as

$$\mathbf{s}' = \mathbf{s} + \tau\hat{\mathbf{p}}, \tag{9.59}$$

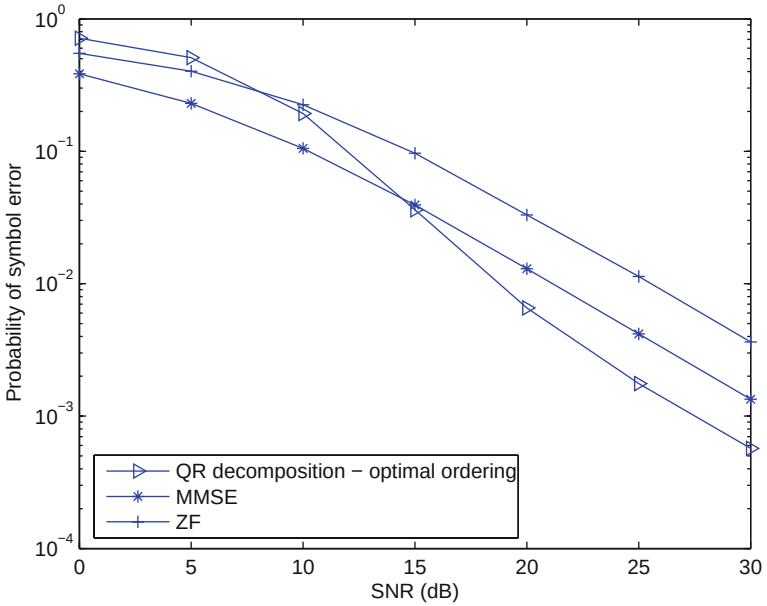

Fig. 9.19 Comparison of the QR decomposition and the linear precoders with $N_T = K = 4$

where the components of the signal vector are taken from a square QAM signal constellation, τ is a real positive number, and $\hat{\mathbf{p}}$ is a K-dimensional vector with complex-valued elements whose real and imaginary components are integers. Hence, for $N_T \geq K$, the transmitted signal vector is

$$\mathbf{x} = \mathbf{A}_T \left(\mathbf{s} + \tau \hat{\mathbf{p}} \right), \tag{9.60}$$

where the matrix $\mathbf{A}_T$ is given as

$$\mathbf{A}_T = \begin{cases} \gamma \mathbf{H} \left(\mathbf{H}\mathbf{H}^H \right)^{-1} & \text{zero-forcing criterion} \\ \gamma \mathbf{H}^H \left(\mathbf{H}\mathbf{H}^H + \beta \mathbf{I} \right)^{-1} & \text{MMSE criterion} \end{cases}. \tag{9.61}$$

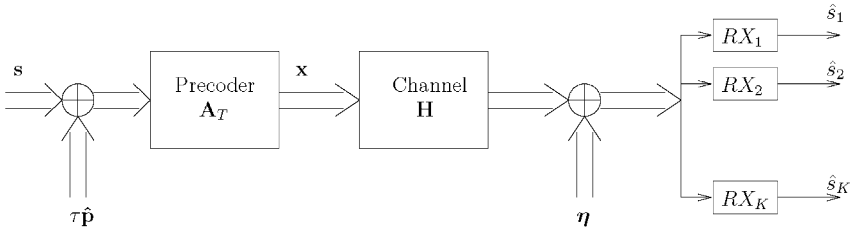

Fig. 9.20 Model of MIMO broadcast system employing vector precoding

The perturbation vector $\hat{\mathbf{p}}$ is chosen to minimize the power in the transmitted signal, i.e.,

$$\hat{\mathbf{p}} = \arg\min_{\mathbf{p}} \|\mathbf{A}_T\,(\mathbf{s} + \tau\mathbf{p})|^2\,, \tag{9.62}$$

subject to the constraint that the real and imaginary components of each element of $\mathbf{p}$ are integers. Methods for solving the least-squares K-dimensional integer-lattice problem and the selection of the positive number τ are described by Hochwald et al. [26].

The received signal vector is

$$\mathbf{r} = \mathbf{H}\mathbf{A}_T\left(\mathbf{s} + \tau\hat{\mathbf{p}}\right) + \boldsymbol{\eta}, \tag{9.63}$$

where $\boldsymbol{\eta}$ is the additive noise vector. Although the perturbation vector $\hat{\mathbf{p}}$ is not known to the receivers, the mth user assumes that its received signal has the form

$$r_m = \gamma\,(s_m + \tau p_m) + \eta'_m, \tag{9.64}$$

where η'_m includes the additive channel noise and the MAI from other users due to the non-zero scale factor β. Since each user knows γ and τ, the mth user performs the modulo operation on the real and imaginary components of r_m to remove p_m and passes the result to its decoder. It is demonstrated in Hochwald et al. [26] that this vector perturbation scheme achieves a signal diversity order comparable to the diversity achieved by the maximum-likelihood detector.

9.4.4 Lattice Reduction Method for Precoding

The lattice reduction method for precoding, described in this section, is similar to the Tomlinson-Harashima precoding for channels with known interference at the transmitter. As in the previous sections, the components of the signal vector to be transmitted are taken from a square QAM signal constellation and, thus, are elements of a lattice.

A lattice can be expressed in terms of its generator matrix $\mathbf{G}$ whose rows denote a basis for the lattice, i.e., all lattice points can be written as a linear combination of the rows of $\mathbf{G}$ with integer weighting coefficients. Any lattice Λ can have many generator matrices and many bases for representation of lattice points. In particular, if $\mathbf{F}$ is a square matrix with integer entries such that $\det(\mathbf{F}) = \pm 1$, then $\mathbf{F}^{-1}$ exists and its entries are all integers. Then, $\mathbf{G}' = \mathbf{G}\mathbf{F}$ is a generator of lattice Λ. The new generator matrix $\mathbf{G}'$ defines a new basis for the lattice Λ. A desirable property of the modified lattice basis is that it be an orthogonal, or close-to-orthogonal basis with the lowest basis vector norms. The process of finding such a basis for a lattice is called *lattice reduction*. Although lattice reduction in high dimensions is an NP-hard problem, a polynomial-time suboptimal lattice reduction algorithm described by Lenstra et al. [29], called the LLL algorithm, gives very good results.

The lattice reduction algorithm developed by Lenstra et al. [29] was designed for real lattices. Gan and Mow [20] have generalized the LLL algorithm to lattices in complex dimensions. Similar to real lattices, if $\mathbf{G}$ is a generator matrix of a complex lattice and $\mathbf{G}' = \mathbf{GF}$, where $\mathbf{F}$ is a square matrix with complex elements having integer real and imaginary parts, such that $\det(\mathbf{F}) = \pm 1$ or $\det(\mathbf{F}) = \pm j$, then $\mathbf{G}'$ is also a basis for the lattice generated by $\mathbf{G}$.

We may apply lattice reduction to the columns of $\mathbf{H}\left(\mathbf{H}\mathbf{H}^H\right)^{-1}$ for the zero-forcing criterion or to the columns of $\mathbf{H}^H\left(\mathbf{H}\mathbf{H}^H + \beta\mathbf{I}\right)^{-1}$ for the MMSE criterion. Thus, we obtain the matrix $\mathbf{F}_{\mathrm{ZF}}$ or $\mathbf{F}_{\mathrm{MSE}}$. For simplicity, let us consider the lattice reduction of the matrix $\mathbf{H}^+ = \mathbf{H}^H\left(\mathbf{H}\mathbf{H}^H\right)^{-1}$, which yields the matrices $\mathbf{F}$ and $\mathbf{F}^{-1}$. The precoding matrix $\mathbf{A}_T$ is given as

$$\mathbf{A}_T = \mathbf{H}^+\mathbf{F}. \tag{9.65}$$

The transmitted signal vector is $\mathbf{x} = \mathbf{A}_T\mathbf{s}'$, where $\mathbf{s}' = \mathrm{mod}_{2\sqrt{M}}[\mathbf{Fs}]$, and the elements of the K-dimensional signal vector $\mathbf{s}$ are selected from an M-ary QAM signal constellation. The received signal vector is

$$\begin{aligned}\mathbf{y} &= \mathbf{Hx} + \boldsymbol{\eta} \\ &= \mathbf{HA}_T\mathbf{s}' + \boldsymbol{\eta} \\ &= \mathbf{Fs}' + \boldsymbol{\eta} \\ &= \mathrm{mod}_{2\sqrt{M}}[\mathbf{s}] + \boldsymbol{\eta}.\end{aligned} \tag{9.66}$$

Thus, each receiver recovers its information symbol without interference from other users.

The lattice reduction technique has been shown to have a performance comparable to that achieved by the vector precoding method described previously. In fact, the signal diversity order achieved by the lattice reduction technique is comparable to the signal diversity order obtained by maximum-likelihood detection, but the lattice reduction technique has a much smaller computational complexity. The interested reader is referred to the papers by Windpassinger et al. [55] and Taherzadeh et al. [46].

9.5 Conclusions

The goal of this chapter was to present an overview of techniques to combat interference in wireless communication systems. We did this by considering typical situations where interference suppression and/or mitigation is necessary to ensure satisfactory system operation, and these examples included both uplink and downlink scenarios. The key waveform designs were single-carrier direct sequence, multicarrier direct sequence, and OFDM, and included both SISO and MIMO systems. The fundamental conclusion to be drawn from the material presented in this

chapter is that many communication systems cannot function in the absence of explicit interference suppression/mitigation procedures, over and above the various modulation and error correction coding techniques that are employed in their design.

References

1. Amihood, P., Masry, E., Milstein, L.B., Proakis, J.G.: Analysis of a MISO pre-BLAST DFE technique for decentralized receivers. In: Proceedings of 40th Asilomar Conference on Signals, Systems and Computers, pp. 1587–1592. Pacific Grove, CA (2006).
2. Amihood, P., Masry, E., Milstein, L.B., Proakis, J.G.: Performance analysis of a pre-BLAST DFE technique for MISO channels with decentralized receivers. IEEE Trans. Commun. **55**, 1385–1396 (2007).
3. Batra, A., Lingam, S., Balakrishnan, J.: Multi-band OFDM: A cognitive radio for UWB. In: Conference Proceedings of IEEE International Symposium on Circuits and Systems (ISCAS), pp. 4094–4097. Island of Kos, Greece (2006).
4. Batra, A., Zeidler, J.R.: Narrowband interference mitigation in OFDM systems. In: Proceedings of the IEEE Military Communications Conference (MILCOM). San Diego, CA (2008).
5. Batra, A., Zeidler, J.R., Beex, A.A.: A two-stage approach to improving the convergence of least-mean square decision-feedback equalizers in the presence of severe narrowband interference. EURASIP J. Adv. Signal Process. (2008). Article ID 390102.
6. Baum, C.W., Pursley, M.B.: Bayesian methods for erasure insertion in frequency-hop communication systems with partial-band interference. IEEE Trans. Commun. **40**, 1231–1238 (1992).
7. Bingham, J.A.C.: Multicarrier modulation for data transmission : An idea whose time has come. IEEE Commun. Mag. **28**, 5–14 (1990).
8. Carron, G., Ness, R., Deneire, L., der Perre, L.V., Engles, M.: Comparison of two modulation techniques using frequency domain processing for in-house networks. IEEE Trans. Consumer Electron. **47**, 63–72 (2001).
9. Chong, L.L., Milstein, L.B.: Comparing DS-CDMA and multicarrier CDMA with imperfect channel estimation. In: Proceedings of 11th IEEE Workshop on Statistical Signal Processing, pp. 385–388. Singapore (2001).
10. Chouly, A., Brajal, A., Jourdan, S.: Orthogonal multicarrier techniques applied to direct sequence spread spectrum CDMA systems. In: Proceedings of the IEEE Global Telecommunications (Globecom) Conference, pp. 1723–1728. Houston (1993).
11. Cimini, L.J.: Analysis and simulation of a digital mobile channel using orthogonal frequency division multiplexing. IEEE Trans. Commun. **COM-33**, 665–675 (1985).
12. Coulson, A.J.: Bit error rate performance of OFDM in narrowband interference with excision filtering. IEEE Trans. Wireless Commun. **5**, 2484–2492 (2006).
13. Da Silva, V.M., Sousa, E.S.: Performance of orthogonal CDMA codes for quasi-synchronous communication systems. In: Proceedings of the IEEE International Conference on Universal Personal Communications (ICUPC), pp. 995–999. Ottawa (1993).
14. Darsena, D.: Successive narrowband interference cancellation for OFDM systems. IEEE Commun. Lett. **11**, 73–75 (2007).
15. Fazel, K., Kaiser, S.: Multi-carrier and Spread Spectrum Systems. John Wiley & Sons, Inc., New York, NY, (2003).
16. Fazel, K., Papke, L.: On the performance of convolutionally-coded CDMA/OFDM for mobile communication systems. In: Proceedings of the IEEE Personal, Indoor, and Mobile Radio Communications (PIMRC) Conference, pp. 468–472. Yokahama (1993).
17. Fischer, R.F.H.: Precoding and Signal Shaping for Digital Transmission. John Wiley & Sons, New York, NY (2002).

18. Fischer, R.F.H., Windpassinger, C., Lampe, A., Huber, J.B.: Space-time transmission using Tomlinson-Harashima precoding. In: Proceedings 4th International ITG Conference on Source and Channel Coding, pp. 139–147. Berlin (2002).
19. Foschini, G.J., Golden, G.D., Valenzuela, R.A., Wolniansky, P.W.: Simplified processing for high spectral efficiency wireless communication employing multi-element arrays. IEEE J. Selected Areas Commun. **17**, 1841–1852 (1999).
20. Gan, Y.H., Mow, W.H.: Accelerated complex lattice reduction algorithm applied to MIMO detection. In: Proceedings of 48th IEEE Global Telecommunications Conference, pp. 2953–2957. St. Louis, MO (2005).
21. Gerakoulis, D., Salmi, P.: An interference suppressing OFDM system for wireless communication. In: IEEE International Conference on Communications (ICC), pp. 480–484. New York, NY (2002).
22. Gray, R.M.: Toeplitz and circulant matrices: A review. Foundations Trends Commun. Inform. Theory **2**, 155–239 (2006).
23. Hara, S., Prasad, R.: Overview of multicarrier CDMA. IEEE Commun. Mag. **35**, 126–133 (1997).
24. Harashima, H., Miyakawa, H.: Matched-transmission technique for channels with intersymbol interference. IEEE Trans. Commun. **COM-20**, 774–780 (1972).
25. Haykin, S.: Adaptive Filter Theory, Fourth edn. Prentice Hall, Upper Saddle River, NJ (2002).
26. Hochwald, B.M., Peel, C.B., Swindlehurst, A.L.: A vector-perturbation technique for near-capacity multiantenna multiuser communication – Part II: Perturbation. IEEE Trans. Commun. **53**, 537–544 (2005).
27. IEEE 802.11: Wireless LAN medium access control (MAC) physical layer (PHY) specifications, amendment 1: High-speed physical layer in the 5 GHz band (1999).
28. Kondo., S., Milstein, L.B.: Performance of multicarrier DS CDMA systems. IEEE Trans. Commun. **44**, 238–246 (1996).
29. Lenstra, A.K., Lenstra, H.W., Lovász, L.: Factoring polynomials with rational coefficients. Math. Ann. **261**, 515–534 (1982).
30. Li, L.M., Milstein, L.B.: Rejection of narrow-band interference in PN spread-spectrum systems using transversal filters. IEEE Trans. Commun. **30**, 925–928 (1982).
31. Li, L.M., Milstein, L.B.: Rejection of CW interference in QPSK systems using decision-feedback filters. IEEE Trans. Commun. **COM-31**, 473–483 (1983).
32. Ling, A.S., Milstein, L.B.: Trade-off between diversity and channel estimation errors in asynchronous MC-DS-CDMA and MC-CDMA. IEEE Trans. Commun. **56**, 584–597 (2008).
33. Milstein, L.B.: Interference Suppression to aid acquisition in direct-sequence spread-spectrum communications. IEEE Trans. Commun. **36**, 1200–1207 (1988).
34. Milstein, L.B., Schilling, D.L., Pickholtz, R.L., Erceg, V., Kullback, M., Kanterakis, E.G., Fishman, D.S., Biederman, W.H., Salerno, D.C.: On the feasibility of a CDMA overlay for personal communications networks. IEEE J. Selected Areas Commun. **10**, 655–668 (1992).
35. Mitola, J., Maguire, G.Q.: Cognitive radio: making software radios more personal. IEEE Personal Commun. Mag. **6**, 13–18 (1999).
36. Nassar, C.R., Natarajan, B., Wu, Z., Wiegandt, D., Zekavat, S.A., Shattil, S.: Multi-carrier Technologies for Wireless Communications. Kluwer Academic Publishers, Boston, MA (2002).
37. Nilsson, R., Sjöberg, F., LeBlanc, J.P.: A rank-reduced LMMSE canceller for narrowband interference suppression in OFDM-based systems. IEEE Trans. Commun. **51**, 2126–2140 (2003).
38. Peel, C.B., Hochwald, B.M., Swindlehurst, A.L.: A vector-perturbation technique for near-capacity multiantenna multiuser communication – Part I: Channel inversion and regularization. IEEE Trans. Commun. **53**, 195–202 (2005).
39. Proakis, J.G.: Digital Communications, Fourth edn. McGraw Hill, Boston, MA (2001).
40. Proakis, J.G., Manolakis, D.G.: Introduction to Digital Signal Processing. MacMillian, New York, NY (1998).
41. Redfern, A.J.: Receiver window design for multicarrier communication systems. IEEE J. Select. Areas Commun. **20**, 1029–1036 (2002).

42. Shensa, M.J.: Time constants and learning curves of LMS adaptive filters. Tech. Rep. 312, Naval Ocean Systems Center, San Diego, CA (1978).
43. da Silva, C.R.C.M.: Performance of spectra-encoded ultra-wideband communication systems in the presence of narrow-band interference. Ph.D. thesis, University of California, San Diego (2005).
44. da Silva, C.R.C.M., Milstein, L.B.: The effects of narrow-band interference on UWB communication systems with Imperfect channel estimation. IEEE J. Select. Areas Commun. **24**, 717–723 (2006).
45. Snow, C., Lampe, L., Schober, R.: Error rate analysis for coded multicarrier systems over quai-static fading channels. IEEE Trans. Commun. **55**, 1736–1746 (2007).
46. Taherzadeh, M., Mobasher, A., Khandani, A.: Communication over MIMO broadcast channels using lattice-basis reduction. IEEE Trans. Inform. Theory **53**, 4567–4582 (2007).
47. Tomlinson, M.: A New Automatic Equalizer Employing Modulo Arithmetic. IEE Electron. Lett. **7**, 138–139 (1971).
48. Tulino, A.M., Verdu, S.: Random Matrix Theory and Wireless Communications. Now Publishers Inc., Boston, MA (2004).
49. Wang, J., Milstein, L.B.: Adaptive LMS filters for cellular CDMA overlay situations. IEEE J. Select. Areas Commun. **14**, 1548–1559 (1996).
50. Wang, T., Proakis, J.G., Masry, E., Zeidler, J.R.: Performance degradation of OFDM systems due to Doppler spreading. IEEE Trans. Wireless Commun. **5**, 1422–1432 (2006).
51. Wang, T., Proakis, J.G., Zeidler, J.R.: Analysis of per-channel equalized filtered multitone modulations over time-varying fading channels. In: Proceedings of the IEEE Personal Indoor and Mobile Radio Communications (PIMRC) (2006).
52. Wang, T., Proakis, J.G., Zeidler, J.R.: Interference analysis of filtered multitone modulation over time-varying fading channels. IEEE Trans. Commun. **55**, 717–727 (2007).
53. Wei, P., Zeidler, J.R., Ku, W.H.: Adaptive interference suppression for CDMA overlay systems. IEEE J. Select. Areas Commun. **12**, 1510–1523 (1994).
54. Weinstein, S.B., Ebert, P.M.: Data transmission by frequency-division multiplexing using the discrete Fourier transform. IEEE Trans. Commun. Technol. **COM-19**, 628–634 (1971).
55. Windpassinger, C., Fischer, R.F.H., Huber, J.B.: Lattice-reduction-aided broadcast precoding. IEEE Trans. Commun. **52**, 2057–2060 (2004).
56. Windpassinger, C., Fischer, R.F.H., Vencel, T., Huber, J.B.: Precoding in multi-antenna and multi-user communications. IEEE Trans. Wireless Commun. **3**, 1305–1316 (2004).
57. Wu, Z., Nassar, C.R.: Narrowband interference rejection in OFDM via carrier interferometry spreading codes. IEEE Trans. Wireless Commun. **4**, 1491–1505 (2005).
58. Yee, N., Linnartz, J.P.: Wiener filtering of multi-carrier CDMA in a Rayleigh fading channel. In: Proceedings of the IEEE Personal, Indoor, and Mobile Radio Communications (PIMRC) Conference, pp. 1344–1347. The Hague (1994).
59. Yee, N., Linnartz, J.P., Fettweis, G.: Multi-carrier CDMA in indoor wireless radio. In: Proceedings of the IEEE Personal, Indoor, and Mobile Radio Communications (PIMRC) Conference, pp. 109–113. Yokahama (1993).
60. Zeidler, J.R.: Performance analysis of LMS adaptive prediction filters. Proc. IEEE **78**, 1781 - 1806 (1990).
61. Zeidler, J.R., Satorius, E.H., Chabries, D.M., Wexler, H.T.: Adaptive enhancement of multiple sinusoids in uncorrelated noise. IEEE Trans. Acoust. Speech, Signal Process. **ASSP-26**, 240 - - 254 (1978).